الجمهورية الجزائرية الديمقراطية الشعبية
People's Democratic Republic of Algeria
وزارة التعليم العالي و البحث العلمي
Ministry of Higher Education and Scientific Research
جامعة أبي بكر بلقايد – تلمسان –
Abou Bekr Belkaid University of Tlemcen
Faculty of Technology

MASTER'S THESIS

Submitted in Partial Fulfillment of the Requirements for the Degree of Master

Field: Mechanical Engineering

Specialty: Renewable Energy

by: BENKOU NAILA
BENKATI BOUCHRA

Title

Study of design and fabrication of an indirect solar dryer

Publicly defended on July 6, 2026, before the examination committee composed of:

Mr. SAIM Rachid	Pr	University of Tlemcen	President
Mr. YOUSFI Sidi Mohammed	MCB	University of Tlemcen	Examiner
Mr. KHELLIL sALIM	Expert	Environmental consulting firm	Socio-economic Representative
Ms. OUARRAD Somia	MCB	University of Tlemcen	I2E Representative
Ms. KHALDI Souheyla	MCA	University of Tlemcen	Supervisor
Mr. GUELLIL Hocine	MCA	University of Tlemcen	Supervisor
Ms. SARI HASSOUN Hind	MAA	University of Tlemcen	Co-supervisor
Mr. KORTI A. Nabil	Pr	University of Tlemcen	Co-supervisor

Academic Year: 2025/2026

Acknowledgements

First and foremost, we thank ALLAH Almighty for giving us the courage, determination, and patience to successfully complete this work under the best possible conditions.

We would like to express our sincere gratitude, first and foremost, to our supervisors: ***Mrs. KHALDI S., and Mrs. SARRI HASSOUN H.****, researchers and lecturers at Abou Bekr Belkaid University of Tlemcen, whose scientific expertise, encouragement, constructive criticism, and moral support guided and assisted us throughout the preparation of this dissertation.*

We would also like to express our sincere gratitude to ***Mr. SAIM R.****, Professor at the University of Tlemcen, for kindly agreeing to preside over the thesis defense committee.*

We also extend our sincere thanks to ***Mr. YOUSFI Sidi Mohammed.****,* ***Ms. OURRAD S****., I2E Representative at the University of Tlemcen, and* ***Mr. KHELLIL S.*** *from Environmental consulting firm for honoring us by accepting to be a member of the defense committee.*

We would also like to extend our deepest thanks to ***Mr. GUELIL H., Mr. KORTI N*** *for the knowledge and guidance they provided throughout our academic journey.*

Finally, we would like to thank all the people who, directly or indirectly, contributed to the completion of this modest work.

Dedication

Naila

I dedicate this modest work to my beloved mother, to whom I owe everything in this life, and to my father, my role model, for his moral support and his presence during difficult times.

To my sisters, ***Yousra*** *and* ***Raghad****, my brother* ***Oussama****, and my niece* ***Israa****.*

To all my teachers who have guided me since my childhood.

And to all those who are dear to me.

Bouchra

I dedicate this modest work to:

My dearest mother,

You are my strength, my light, and my refuge. No words can truly express the immense love and gratitude I have for you. This work is, above all, yours.

My dear father,

For your support, kindness, and encouragement. Thank you for always believing in me.

My beloved brothers, ***Mohamed, Ayoub, Yacine,*** *and* ***Zakaria****,*

My dear sisters, ***Amina*** *and* ***Amira****,*

*My teachers and professors****,***

From primary school to the completion of this thesis

To all those I love and who believed in me,

Thank you for your support, trust, and encouragement.

Abstract

This work presents an experimental investigation of an indirect forced-convection solar dryer incorporating an innovative active-wall concept, in which the sun-facing wall of the drying chamber is replaced by a wall-integrated flat-plate air solar collector, enabling the recovery of solar energy otherwise lost through the dryer envelope. Two absorber configurations were tested: a flat-plate absorber and a tubular absorber integrating parallel rough-surfaced aluminium tubes. Laboratory tests demonstrated that the tubular configuration achieves a superior thermal efficiency of 72% versus 68% for the flat-plate design, with a more uniform temperature distribution and a broader optimal operating range. The complete solar drying system comprising the primary collector coupled with the active-wall chamber was subsequently tested outdoors at the University of Tlemcen in June, under real solar irradiance conditions, using banana slices and mint leaves as drying products. Outdoor experiments confirmed the operational feasibility of the system, with the primary collector delivering outlet temperatures of 54 °C and 72 °C for the flat-plate and tubular configurations respectively. However, the wall-integrated secondary collector exhibited a limited thermal contribution under the current serial airflow arrangement, as the pre-heated air arriving from the primary collector frequently exceeded the secondary absorber temperature, resulting in a net heat loss. A circuit inversion ($T_{amb} \rightarrow C_2 \rightarrow C_1 \rightarrow$ chamber) is proposed as a priority design improvement to address this limitation.

Keywords: drying, indirect dryer, solar collector, forced-air drying, drying kinetics, banana and mint.

Résumé

Ce travail présente une étude expérimentale d'un séchoir solaire indirect à convection forcée intégrant un concept innovant de paroi active, dans lequel la paroi exposée au soleil de la chambre de séchage est remplacée par un capteur solaire plan à air intégré directement à la paroi, permettant la récupération de l'énergie solaire autrement perdue à travers l'enveloppe du séchoir. Deux configurations d'absorbeur ont été testées : un absorbeur plan lisse servant de configuration de référence, et un absorbeur tubulaire intégrant un réseau de tubes en aluminium à surface rugueuse disposés en parallèle. Les essais en laboratoire ont démontré que la configuration tubulaire atteint un rendement thermique supérieur de 72% contre 68% pour l'absorbeur plan, avec une distribution de température plus uniforme le long de la surface absorbante et une plage de fonctionnement optimal plus large. Le système de séchage solaire complet comprenant le capteur principal couplé à la chambre à paroi active a ensuite été testé en extérieur à l'Université de Tlemcen au mois de juin, sous rayonnement solaire réel, en utilisant des tranches de banane et des feuilles de menthe comme produits à sécher. Les expériences en extérieur ont confirmé la faisabilité opérationnelle du système, le capteur principal délivrant des températures de sortie de 54 °C et 72 °C pour les configurations à absorbeur plan et tubulaire respectivement. Cependant, le capteur secondaire intégré à la paroi a présenté une contribution thermique limitée dans la configuration actuelle d'écoulement en série, l'air préchauffé provenant du capteur principal dépassant fréquemment la température de l'absorbeur secondaire, entraînant une perte thermique nette. Une inversion du circuit (T_{amb} → C_2 → C_1 → chambre) est proposée comme amélioration prioritaire pour remédier à cette limitation.

Mots-clés : séchage, séchoir indirect, capteur solaire, séchage à air forcée , cinétique de séchage, banane et menthe.

الملخص

تقدم هذه الدراسة تحقيقًا تجريبيًا لمجفف شمسي غير مباشر بالحمل الحراري القسري، يتضمن مفهومًا مبتكرًا يُعرف بـ"الجدار النشط، حيث يتم استبدال الجدار المواجه للشمس في غرفة التجفيف بمجمع شمسي مستوٍ للهواء مدمج مباشرةً في الجدار، مما يتيح استرداد الطاقة الشمسية التي كانت تُفقد عبر غلاف المجفف. تم اختبار تصميمين مختلفين للماص :ماص مستوٍ أملس يمثل التصميم المرجعي، وماص أنبوبي يضم مجموعة من الأنابيب الألومينيوم ذات السطح الخشن المرتبة

بشكل متوازٍ. أثبتت الاختبارات المخبرية أن التصميم الأنبوبي يحقق كفاءة حرارية أعلى بلغت 72%مقارنةً بـ 68%

للتصميم المستوي، مع توزيع أكثر انتظامًا لدرجات الحرارة على طول سطح الماص ونطاق تشغيل مثالي أوسع. وقد خضع نظام التجفيف الشمسي الكامل — المكوّن من المجمع الرئيسي المقترن بغرفة الجدار النشط — لاختبارات ميدانية في جامعة تلمسان خلال شهر جوان، تحت ظروف الإشعاع الشمسي الحقيقي، باستخدام شرائح الموز وأوراق النعناع منتجات للتجفيف. أكدت التجارب الميدانية الجدوى التشغيلية للنظام، إذ حقق المجمع الرئيسي درجات حرارة عند المخرج بلغت

درجة 54°C و 72 °C للتصميمين المستوي والأنبوبي على التوالي. غير أن المجمع الثانوي المدمج في الجدار أظهر مساهمة حرارية محدودة في التكوين الحالي للتدفق التسلسلي، إذ كانت درجة حرارة الهواء المسخّن مسبقًا القادم من المجمع الرئيسي تتجاوز في أغلب الأحيان

حرارة الماص الثانوي، مما أدى إلى فقدان حراري صافٍ. ولمعالجة هذه المحدودية، يُقترح عكس دائرة تدفق الهواء ($T_{amb} \rightarrow C_2 \rightarrow C_1$)

غرفة التجفيف كتحسين تصميمي ذي أولوية.

.الكلمات المفتاحية: التجفيف، المجفف غير المباشر، المجمع الشمسي، التجفيف بالهواء القسري، حركية التجفيف، الموز والنعناع

Table of Contents

Abstract ii
Table of Contents iii
List of Figures iv
List of Tables v
Nomenclature vi

General Introduction 1

CHAPTER I: General Concepts of Drying

I.1. Introduction 5
I.2. General information about drying 5
I.2.1. Definition 5
I.2.2. Objective of drying 5
I.2.3. Advantages and limitations of drying 6
I.3. Characteristics of drying air 6
I.3.1. Relative Humidity 6
I.3.2. Absolute humidity (or specific humidity) 6
I.4. Characterization of moist solids 7
I.4.1. Absolute Humidity 7
I.4.2. Relative Humidity 7
I.4.3. Water Activity 7
I.5. Physical phenomena occurring in the product during convection drying 8
I.6. Drying kinetics 8
I.7. Drying rate 10
I.8. Thermal efficiency of solar collector η
I.9. Drying Methods 10
I.9.1. Natural Drying 10
I.9.2. Artificial Drying 11
I.10. Drying method 11
I.10.1. Direct solar dryer 11
I.10.2. Indirect solar dryer 12
I.10.3. Mixed solar dryer 13
I.10.4. Hybrid solar dryers 14
I.11. Conclusion 14

CHAPTER II: Bibliographic Review

II.1. Introduction 16
II.2. Integration of Thermal Energy Storage Using Phase Change Materials (PCM) 16
II.2.1. Indirect forced convection dryer with MCP integrated into the sensor 16
II.2.2. Active indirect dryer with conical MCP and photovoltaic panels 17
II.3. Energy, Exergy and Techno-Economic Analyses 18
II.3.1. Comparison of hybrid dryer, indirect dryer, and shade drying 18
II.3.2. Energy and exergy analysis of an indirect dryer for oranges 19
II.4. Integration of Smart Technologies (IoT and Artificial Intelligence) 20
II.4.1. Predictive control of an indirect forced convection dryer 20
II.4.2. Connected indirect dryer for temperate crops 21
II.5. Optimization of Structural Configurations and Design Variants 22
II.5.1. Indirect forced convection dryer integrating a silica gel dehumidifier 22
II.5.2. Double-sided absorber indirect solar dryer for vegetables 23
II.6. Drying Kinetics and Product Quality 24
II.6.1. Drying Kinetics and Mathematical Modeling 24
II.6.2. Drying of Apple Slices: Multi-Condition Evaluation 25
II.7. Conclusion 26

CHAPTER III: Materials and Methods

III.1. Introduction 28
III.2. Description of the Solar Dryer Prototype 28
III.2.1. General Structure of the Dryer 28
III.2.2. Solar simulator 29
III.2.3. Solar Thermal Collector 30
III.2.4. Drying Chamber 31
III.2.5. Air Circulation System 32
III.3. Assembly Components 32
III.4. Assembly of the Drying Chamber and the Solar Collector 34
III.4.1. Solar Thermal Collector 34
III.4.2. Drying Chamber 35
III.4.3. General View of the Assembled Prototype 35
III.5. Instrumentation and Measuring Instruments 36

III.5.1. Measurement of Solar Radiation 36
III.5.2. Temperature Measurement 37
III.5.3. Air Velocity Measurement 38
III.5.4. Mass Measurement 39
III.6. Incorporation of flexible metal pipes into the collector 39
III.7. Experimental Methodology 40
III.8. Conclusion 41

CHAPTER IV: Experimental results

IV.1. Introduction 44
IV.2. Solar Dryer with a Flat-Plate Collector 44
IV.2.1. Thermal Behavior Analysis 45
IV.2.1. Thermal efficiency of the collector 46
IV.2.2. Effect of flow rate variation at constant irradiance (I = 330 W/m²) 49
A. Absorber temperature 49
B. Solar collector heat gain of ($T_{in,d} - T_{amb}$) 50
C. Thermal efficiency of the solar collector 51
IV.2.3. Effect of irradiance variation at constant flow rate ($\dot{m}$ = 0.015 kg/s) 53
A. Absorber temperature 53
B. Solar collector heat gain ($T_{in,d} - T_{amb}$) 54
C. Thermal efficiency of the solar collector 55
IV.3. Solar Dryer with a metallic tubular absorber 57
IV.3.1. Comparative Thermal Performance Analysis of a Flat-Plate Absorber and an Absorber with Tubes 58
A. Absorber temperature 58
B. Thermal efficiency 59
C. Effect of radiations 60
D. Effect of mass flow rate 61
IV.4. Summary of key performance indicators for both configurations 63
IV.5. Conclusion 64

CHAPTER V: Results and discussions

V.1. Introduction 67
V.2. Description of the complete solar drying system 67

V.3. Measuring Devices and Instruments 69
V.4. Organization of Experimental Tests 69
V.5. Experimental Results 70
V.5.1. Climatic Conditions 70
V.6. Thermal behavior analysis of the solar dryer 71
V.6.1. Solar dryer without tubes (day 1) 72
V.6.2. Solar dryer with tubes (day 2) 73
V.7. Evolution of Product Mass 75
A. Banana 75
B. Mint 76
V.8. Product after drying 77
V.9. Conclusion 78

List of Tables

CHAPTER IV: Results and Discussion

Table IV. 1: A comparison of the absorber temperatures between the two configurations..... 58
Table IV. 2**:** Summary of key performance indicators for both configurations..... 63

CHAPTER V: Results and Discussion

Table V.1**:** Appearance of the dried products under the three drying conditions 77

List of figures

CHAPTER I: General Concepts of Drying

Figure I. 1. Dried fruits and vegetables 5
Figure I. 2. Variation of product (X) moisture content over time 9
Figure I. 3. Three-phase drying kinetics 9
Figure I. 4. Direct solar dryer 12
Figure I. 5. Indirect solar dryer 13
Figure I. 6. Mixed solar dryer 13
Figure I. 7. Hybrid solar dryers 14

CHAPTER II: Bibliographic Review

Figure II. 1. Experimental setup: (a) Front view of the drying chamber with tray and dried lemongrass sample, (b) detailed schematic diagram of the drying chamber with the dimensions, (c) image of the whole experimental setup along with all the measuring instruments 17
Figure II. 2. Experimental setup. 18
Figure II. 3. Schematic diagram of the experimental setup for a solar dryer and hybrid dryer system with instrumentation and control components 19
Figure II. 4. A photograph of the solar dryer 20
Figure II. 5.Séchoir solaire indirect à convection forcée pour le séchage de tomates cerises .. 21
Figure II. 6.Constructed model of the indirect solar dryer for practical use 22
Figure II. 7. Experimental setup of a PV-powered indirect solar dryer: outdoor installation and instrumented drying chamber loaded with tomato slices 23
Figure II. 8. Different parts of solar dryer 24
Figure II. 9. The indirect solar dryer used for the drying experiments 25
Figure II. 10. Experimental setup of a PV-powered indirect solar dryer: (a) full system view with labeled components, (b) close-up of internal fans and drying sample 26

CHAPTER III: Materials and Methods

Figure III. 1: (a) The fabricated solar dryer prototype, (b) simplified schematic of the prototype 29
Figure III. 2: Solar simulator 30
Figure III. 3: Schematic diagram of the solar thermal collector, (a) Side view, (b) front view of absorber. Thermocouple positions 30

Figure III. 4: Schematic diagram of the drying chamber, (a) Side view, (b) top view. Thermocouple positions..... 31
Figure III. 5: OPSSING electric fan used for forced air circulation..... 33
Figure III. 6: Matte black painted metal sheet (absorber), plywood panel and glass..... 34
Figure III. 7: PROSEAL sealant used for glass cover sealing..... 34
Figure III. 8: Final view of the solar collector..... 36
Figure III. 9. Experimental setup in the laboratory: solar simulator facing the solar collector and drying chamber..... 37
Figure III. 10. Solarimeter..... 38
Figure III. 11: Thermocouples type K..... 38
Figure III. 12: Data Logger..... 39
Figure III. 13: Thermo-anemometer..... 39
Figure III. 14: electronic Balance..... 40
Figure III. 15: (a) flexible metal pipes, (b) integration of pipe into the collector..... 41

CHAPTER VI: Results and discussions

Figure IV. 1: Temporal variation of the temperatures measured in the solar collector (T_1, T_2, and T_3) and the drying chamber ($T_{in,\,d}$, T_5, and $T_{out,\,d}$)..... 46
Figure IV. 2: Temporal evolution of thermal efficiency of the collector..... 47
Figure IV. 3: Effect of air mass flow rate on the temporal evolution of the collector temperature T_2..... 50
Figure IV. 4: Variation of the collector thermal gain with time at different mass flow rates..... 51
Figure IV. 5: Effect of air mass flow rate on the thermal efficiency of the flat-plate solar collector (ηL)..... 52
Figure IV. 6: Effect of solar irradiance on the temporal evolution of the collector temperature T_2..... 53
Figure IV. **7**: Temporal evolution of the collector thermal gain under different solar irradiance levels..... 55
Figure IV. 8: Variation of the thermal efficiency (η_L) as a function of solar irradiance..... 56
Figure IV. 9: Comparison of the thermal efficiency of the smooth flat-plate collector and the tubular absorber collector..... 59
Figure IV. 10: Variation of collector thermal efficiency with air mass flow rate for the two absorber configurations..... 60
Figure IV. 11: Variation of collector thermal efficiency with solar irradiance for the two absorber configurations..... 61

CHAPTER VI: Results and discussions

Figure V. 1: General view of the solar dryer installed under real conditions..... 67
Figure V. 2: Banana slices and mint leaves arranged on the trays before drying..... 68
Figure V. 3: Evolution of solar radiation during the two Experiments..... 70
Figure V. 4: Evolution of ambient temperature during the two experiments..... 71

Figure V. 5: Temporal evolution of the temperature of the different components of the solar dryer without tubes 72
Figure V. 6: Temporal evolution of the temperature of the different components of the solar dryer with tubes (day 2) 73
Figure V. 7: Hourly Evolution of the mass of bananas during the drying process 75
Figure V. 8: Hourly Evolution of the mass of mint during the drying process 76

Nomenclature

Latin letters		**Unit**
A_c	Collector surface area	m^2
C_p	Specific heat	
I	incident solar radiation	W / m^2
$\dot{m}$	Mass flow rate	kg/s
M_e	Water mass	kg
M_h	Wet material mass	kg
M_s	Dry matter mass	kg
T	Temperature	°C
t	Time	h/min
V	Wind speed	m / s
X	Humidity	
X_r	Moisture content	

Greek symbols

η	Efficiency

Subscripts

amb	Ambient
in,d	Chamber inlet
out,d	Chamber outlet

General Introduction

Solar energy is one of the most viable renewable energy sources, owing to its continuous availability and non-polluting nature, unlike fossil fuels, which exist in limited quantities. In the context of global population growth and rising food needs, preserving agricultural products and reducing post-harvest losses have become essential to ensuring food security.

Drying is one of the oldest and most effective preservation methods: it lowers the moisture content of the product, extends its shelf life, and facilitates storage and transport. While traditional open-air drying remains widespread, it suffers from slow processing times and exposes the product to contamination, whereas electric dehydrators consume large amounts of energy. Solar drying therefore stands out as an economical and efficient alternative, combining speed with product quality.

The principle relies on heating air through a solar collector, which is then directed toward the drying chamber by natural or forced convection. Among the existing configurations, the indirect dryer stands out by shielding the product from direct sun exposure, thereby preserving its color and nutritional value.

This study presents an experimental investigation of an indirect forced-convection solar dryer designed for the drying of agricultural products in small quantities. The drying chamber consists of four lateral walls, one of which directly faces the incident solar radiation during operation. In conventional designs, this sun-facing wall is typically constructed from wood the same material used for the remaining walls and therefore acts as a thermally inert surface that absorbs solar radiation without contributing any useful thermal energy to the drying process, resulting in a significant and systematic loss of exploitable radiative energy.

The central innovation of this work consists in replacing this conventional wooden wall with an integrated flat-plate air solar collector, directly affixed to the sun-facing surface

of the drying chamber, effectively transforming an otherwise passive wall into an active thermal component. In this enhanced configuration, the air stream delivered by the primary solar collector does not enter the drying chamber directly; instead, it first passes through this wall-integrated secondary collector, where it undergoes an additional stage of thermal elevation before being introduced into the drying space. This serial thermal arrangement allows the system to recover and valorize the solar energy that was previously lost through the sun-facing wall, providing supplementary heating to the drying air without requiring any additional energy input or increase in collector surface area external to the dryer.

The originality of this approach lies in the dual functional role assigned to the sun-facing wall: it simultaneously serves as a structural envelope component and as an active solar energy conversion surface, seamlessly integrated into the existing architecture of the dryer. This concept of an absorber-wall coupling represents a compact, low-cost, and thermally efficient design strategy for enhancing the performance of small-scale solar drying systems, particularly in contexts where available surface area and material resources are limited.

In order to assess the influence of the absorber geometry on the thermal performance of the wall-integrated collector, two distinct absorber configurations were experimentally investigated and compared. The first configuration consists of a conventional flat-plate absorber a smooth surface baseline design while the second incorporates an array of parallel rough-surfaced metallic tubes directly integrated onto the absorber surface. This comparative approach aims to evaluate the extent to which the tubular geometry, by increasing the effective heat exchange area and promoting local flow turbulence, can enhance convective heat transfer between the absorber and the working fluid relative to the conventional flat-plate design.

This master's thesis is organized into five chapters. The first presents general background on drying and its basic principles. The second offers a literature review focused specifically on indirect solar dryers, their operating principles, and prior work carried out in this field. The third describes the materials and methods used to design and build the prototype. The fourth presents and discusses the results of the experimental tests carried out

for the active wall collector under controlled laboratory conditions, using a solar simulator as the radiation source. The fifth chapter presents the results of outdoor experimental tests conducted under real climatic conditions, in which the complete solar drying system comprising the primary collector coupled with the active-wall chamber was evaluated under natural solar irradiance, providing a comprehensive assessment of the overall thermal and drying performance of the integrated prototype. The thesis concludes with a general conclusion summarizing the key findings and outlining perspectives for future work.

CHAPTER I

Generalities of Drying

Table of contents

I.1. Introduction 5
I.2. General information about drying 5
I.3. Characteristics of drying air 6
I.4. Characterization of moist solids 7
I.5. Physical phenomena occurring in the product during convection drying 8
I.6. Drying kinetics 8
I.7. Drying rate 10
I.8. Drying Methods 10
I.9. Drying method 12
I.10. Conclusion 14

I.1. Introduction

Solar energy is an important renewable source that has long been used in various fields. Among its applications, solar drying is a simple method that uses sunlight to remove moisture from products in order to preserve them longer. This technique, ancient yet still in use today, constitutes an economical and ecological solution for the preservation of food and other materials. In this chapter, we will briefly present the principles of solar drying as well as its main advantages and application (Figure I. 1.).



Figure I. 1. Dried fruits and vegetables.

I.2. General information about drying

I.2.1. Definition

Drying is a unit operation that consists of partially or completely removes water from a moist object through evaporation. This operation is achieved through several methods such as evaporation, heating, or exposure to air, etc. The purpose of drying is to ensure the preservation of products by reducing their water content, which can otherwise alter some of their properties (taste, texture, quality, etc…).

I.2.2. Objective of drying

Drying consists of removing the water contained in a material through the application of heat. This process limits the growth of microorganisms and slows down the decomposition of products. It therefore ensures better preservation and longer storage under normal conditions.

I.2.3. Advantages and limitations of drying

❖ **Advantages of Drying**

- Easy to implement and effective.
- Extends the shelf life of food products significantly
- Eliminates bacteria and deactivates enzymes.
- Reduces post-harvest wastes.
- Reduces transportation costs due to lower weight

❖ **Limitations of drying**

- The surface of products may become hard and dry, making rehydration difficult
- Consumes a lot of energy so expensive**.**

I.3. Characteristics of drying air

I.3.1. Relative Humidity

Also called hygrometric degree, relative humidity corresponds to the ratio between the partial pressure of water vapor present in the air and the saturation vapor pressure at the same temperature. It is expressed by the following relationship:

$$\boldsymbol{H_r} = \frac{P_V}{P_{sat}} \qquad \text{(I.1)}$$

$\boldsymbol{P_v}$: Is the partial pressure of water vapor,

$\boldsymbol{P_{sat}}$: Is the saturation pressure of water vapor at the temperature considered.

I.3.2. Absolute humidity (or specific humidity)

Absolute humidity, also called specific humidity, is defined as the ratio between the mass of water vapor contained in a volume of humid air and the mass of dry air present in the same volume. It is expressed as:

$$H_a = \frac{m_v}{m_a} \qquad \text{(I.2)}$$

m_v: is the mass of water vapor,

m_a: is the mass of dry air.

Assuming that dry air and water vapor behave as ideal gases, this relationship can be written in terms of partial pressures:

$$H_a = 0{,}622 \ \frac{P_v}{P - P_v} \qquad \text{(I.3)}$$

I.4. Characterization of moist solids

I.4.1. Absolute Humidity

The absolute humidity of a solid, also called water content or moisture content on a dry basis, represents the amount of liquid present in the wet solid relative to the mass of the dry solid. It is expressed by the following equation:

$$H_a = \frac{M_l}{M_s} = \frac{M_h - M_s}{M_s} \quad \text{(I.4)}$$

M_l is the mass of the liquid (kg)

M_h is the mass of the wet solid (kg),

M_s is the mass of the dry solid (kg).

I.4.2. Relative Humidity

The relative humidity of solid, also called moisture content on a wet basis corresponds to the ratio of the mass of the liquid contained in the solid to its total wet mass:

$$H_r = \frac{M_l}{M_h} = \frac{M_h - M_s}{M_h} \quad \text{(I.5)}$$

M_l is the mass of the liquid (kg)

M_h is the mass of the wet solid (kg)

M_S is the mass of the dry solid (kg)

I.4.3. Water Activity

Water activity, denoted by (a_w), refers to the amount of free water available in a product. It should not be confused with moisture content, which represents the total quantity of water contained in the material. Indeed, part of the water may be bound to the product's constituents and therefore unavailable for transfer or evaporation. Water activity characterizes only the water that can evaporate or participate in moisture transfer. It is defined as the ratio between the water vapor pressure of the product and that of pure water at the same temperature:

$$a_w = \frac{P_v}{P_s} \quad \text{(I.6)}$$

where (P_v) is the vapor pressure above the product and (Ps) is the vapor pressure above pure water at the same temperature. The values of (a_w) range from 0 to 1; the higher the value, the greater the amount of free water available in the product [1].

I.5. Physical phenomena occurring in the product during convection drying

During convective drying, three main physical phenomena occur simultaneously at the surface and inside the product.

- **Heat transfer**

Hot air flows over the product and transfers heat to it. This heat then penetrates into the product through three mechanisms: conduction through the material, convection due to the movement of water inside the product, and phase change when water turns into vapor. The greater the temperature difference between the air and the product, the faster the heat transfer.

- **Mass transfer**

The heat received causes the water contained in the product to evaporate. The water vapor generated leaves the product and is carried away by the moving air. This process continues as long as the product contains more moisture than the surrounding air. The difference in moisture content between the product and the air is what drives this transfer.

- **Internal water diffusion**

Inside the product, water naturally moves from wetter regions toward drier regions until it reaches the surface, where it evaporate. The faster this internal diffusion occurs, the more efficient the drying process becomes.

These three phenomena operate together: heat causes evaporation, evaporation drives mass transfer, and internal diffusion continuously replenishes the water at the product surface [2].

I.6. Drying kinetics

The drying kinetics of products are analyzed through graphs that illustrate how the drying rate changes over time. These curves are obtained by conducting experimental tests under varying conditions such as ambient temperature, relative humidity, and the velocity of the drying air. They provide a comprehensive view of the product's behavior throughout the drying process, highlighting the influence of different factors on the gradual reduction of moisture content. As such, these curves serve as essential tools for understanding and optimizing the moisture transfer mechanisms during drying.

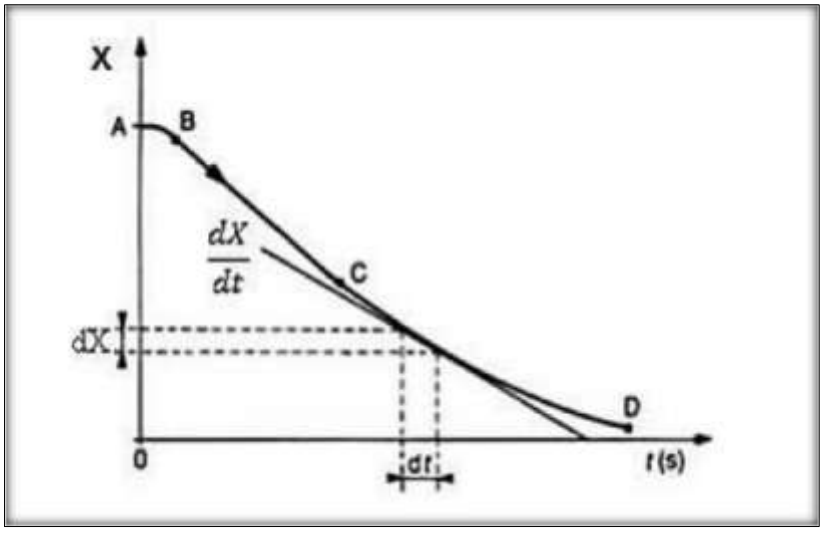


Figure I. 2. Variation of product (X) moisture content over time.

From the curve presented in figure I.2. It is possible to plot the following curve figure I.3.

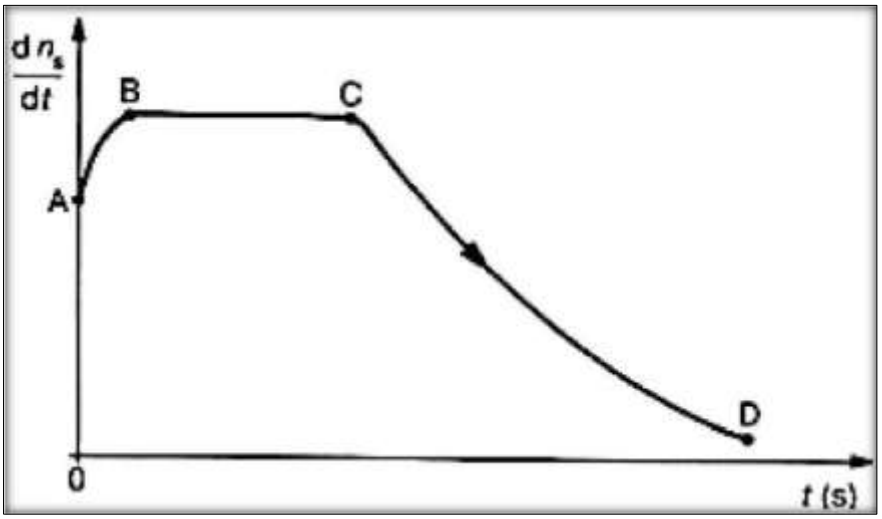


Figure I. 3. Three-phase drying kinetics

• Heating phase [AB]:

This phase corresponds to the initial heating of the product. Its temperature gradually increases, leading to an acceleration of the drying rate until a state of thermal equilibrium are reached.

• Constant drying rate phase [BC]:

During this stage, the free water on the surface of the product evaporates continuously and is replenished by water migrating from within. The drying rate remains constant, and the product temperature remains stable.

• Decreasing drying rate phase [CD]:

This phase begins once the free water has been depleted. Drying then affects the bound water, the transfer of which to the surface becomes increasingly difficult. An evaporation front progresses towards the interior of the product, causing a slowing of the drying rate. Consequently, the product temperature gradually increases and tends to approach that of the drying air [3].

I.7. Drying rate

The drying air represents the amount of water evaporated from a product per unit of time. It is generally expressed by the relation:[4]

$$V=\frac{dx}{dt} \quad (I.7)$$

where x represents the moisture content of the product and (t) the drying time. This quantity reflects the decrease in moisture content over time and allows characterization of the heat and mass transfer phenomena occurring during drying [4]. The drying rate depends on several parameters related to the nature of the material, such as porosity, shape, and initial moisture content, as well as operating conditions such as the temperature, humidity, and velocity of the drying air. Its study is essential for analyzing the kinetics of the process and optimizing drying performance.

I.8. Thermal efficiency of solar collector η

The thermal efficiency η of the solar collector is defined as the ratio of the useful heat transferred to the working fluid to the total incident radiative flux received by the absorber surface. It constitutes the primary performance indicator of the collector, quantifying the effectiveness of the energy conversion process and reflecting the combined influence of the convective heat transfer conditions, the absorber surface properties, and the magnitude of thermal losses to the surroundings.

$$\boldsymbol{\eta} = \frac{m*cp*(T_{out}-T_{in})}{I*A_W}$$

I.9. Drying methods

I.9.1. Natural Drying

Natural drying is the oldest technique, practiced for generations. It uses natural climatic conditions as an energy source to remove moisture from products. Two main types can be distinguished:

a) Open-air drying: This method consists of exposing the product to ambient air without any additional heat input. The product is simply spread outdoors and water evaporation occurs naturally through wind and the heat of the surrounding air. Although very simple and cost-free, this method is extremely slow and exposes the product to external contamination such as dust, insects, and bacteria, which can considerably alter the quality of the final product.

b) Sun drying: This is the most widespread natural method. It consists of exposing the product directly to sunlight by spreading it on mats or racks on the ground. Solar radiation provides the heat necessary for vaporizing the water contained in the product. Although more effective than open-air drying, this method presents numerous drawbacks: long drying times, exposure of the product to dust, rain, and insects, as well as the risk of rotting and mold that can affect up to 50% of harvests. Furthermore, direct exposure to solar radiation can cause vitamin degradation and discoloration of the product.

I.9.2. Artificial Drying

Faced with the limitations of natural drying, artificial dryers were developed from the 20th century onward based on rigorous scientific principles. Artificial drying involves a double transfer: a heat transfer intended to reduce the moisture content of the product, and a mass transfer involving the movement of water from the interior of the product to its surface. Both transfers require a considerable heat input, which can be supplied by different methods:

a) Convective drying: This is the most widely used method in the food industry. Heat is supplied to the product by a flow of hot air that circulates around the product and carries away the evaporated water vapor. A dryer is said to be of the convective type when energy is supplied to the product by heated air. This drying mode allows good control of temperature and air velocity, which promotes uniform and rapid evaporation of water.

b) Conductive drying: In this case, heat is transferred to the product by direct contact with a heated surface. A dryer is classified as conductive when heat is transmitted directly to the product without a gaseous intermediary. This method is particularly suited to liquid or pasty products and allows very efficient heat transfer.

c) Radiation drying: Heat is supplied to the product by infrared radiation or high-frequency electromagnetic waves, without direct contact between the heat source and the product. This drying mode allows rapid and uniform heating of the product in depth, which considerably reduces drying times and better preserves the nutritional quality of the treated products.

I.10. Drying method

I.10.1. Direct solar dryer

In this type (Figure.I.4), solar radiation passes directly through a transparent cover and dries the product placed inside the drying chamber. It is a simple system and more efficient than open-air sun drying, however, it is limited to small quantities. Additionally, direct exposure to sunlight can cause color changes and nutrient degradation in the product. Moisture condensation on the glass can also reduce its transmissivity**.**

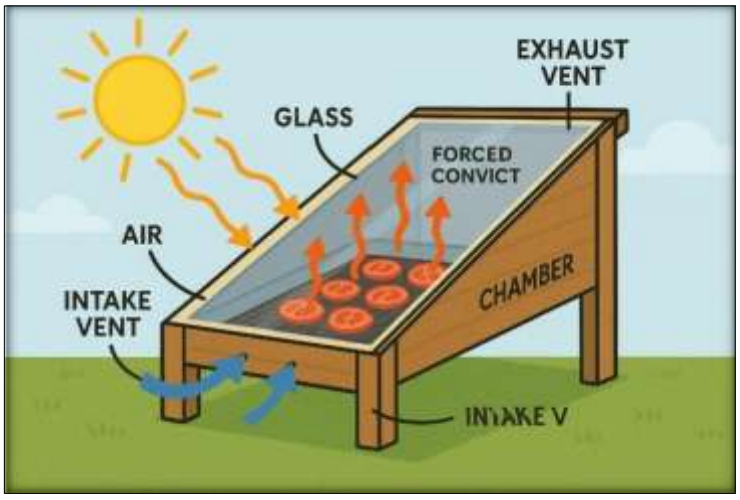


Figure I. 4. Direct solar dryer

I.10.2. Indirect solar dryer

In this type (Figure.I.5.), the solar collector is separated from the drying chamber. The air is first heated by the collector and then directed into the chamber to dry the product. Therefore, the product is never directly exposed to sunlight. This allows better product quality, a more stable temperature, and reduced photochemical damages. This type is particularly suitable for sensitive products such as citrus fruits.

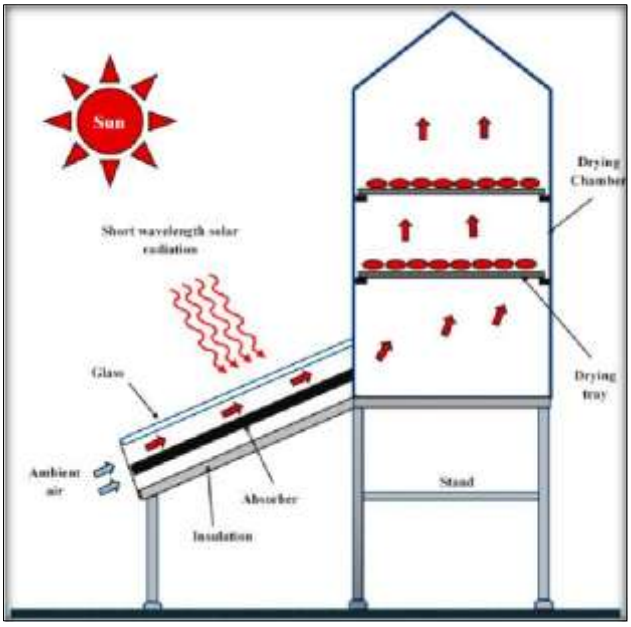


Figure I. 5. Indirect solar dryer

I.10.3. Mixed solar dryer

Mixed solar dryers (Figure I.6.) combine the principles of direct and indirect dryers to improve drying efficiency. They use both direct solar radiation on the product and air preheated by a solar collector to provide the necessary heat. Their structure is similar to that of indirect dryers, consisting of a solar collector, a drying chamber, and a chimney; however, the glazed walls also allow solar radiation to reach the product directly.

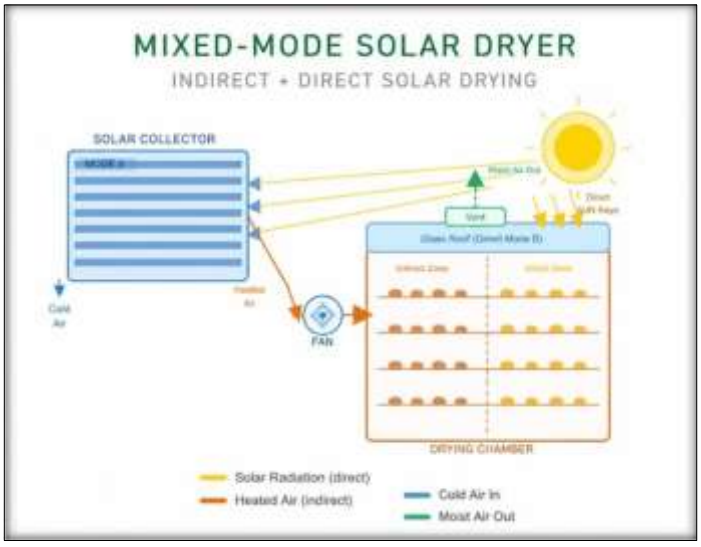


Figure I. 6. Mixed solar dryer

I.10.4. Hybrid solar dryers

Hybrid dryers (figure. I.1.) combine solar energy with auxiliary energy sources such as electricity, fuel oil, or biomass to ensure continuous and efficient drying. Solar energy is mainly used to preheat the air, while the backup sources maintain a stable temperature regardless of weather conditions. Although more costly, these systems are suitable for industrial and large-scale applications, ensuring good product quality and high final yield.

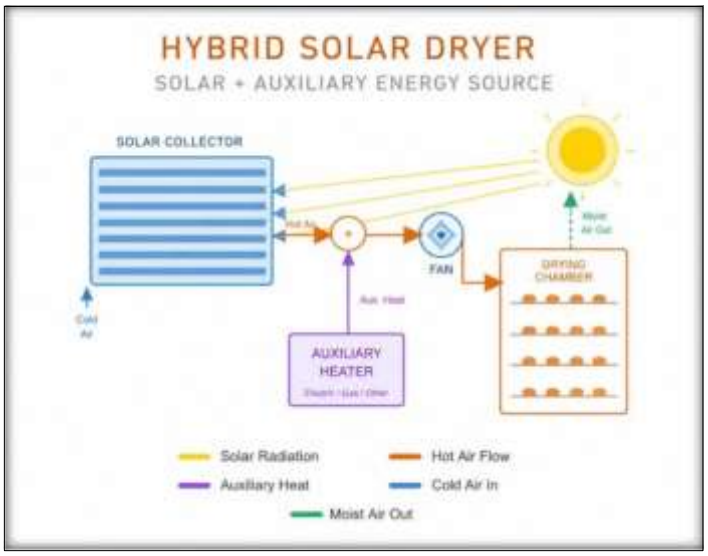


Figure I. 7. Hybrid solar dryers

I.11. Conclusion

This chapter presented the fundamentals of drying and highlighted its importance in preserving food products. Several parameters influence drying efficiency, including temperature, humidity, and air velocity. The main drying methods were discussed, including open air drying, conduction drying, convection drying, and radiation drying. A classification of solar dryers (direct, indirect, mixed and hybrid) was also provided. This chapter serves as a basis for understanding how to select the appropriate solar dryer for a given application.

CHAPTER II

Bibliographic Review

Table of Contents

II.1. Introduction 16
II.2. Integration of Thermal Energy Storage Using Phase Change Materials (PCM) 16
II.3. Energy, Exergy and Techno-Economic Analyses 18
II.4. Integration of Smart Technologies (IoT and Artificial Intelligence) 20
II.5. Optimization of Structural Configurations and Design Variants 22
II.6. Drying Kinetics and Product Quality 24
II.7. Conclusion 26

II.1. Introduction

This chapter represents the scientific contributions made by researchers in the field of solar drying worldwide. Exploring the evolution of scientific research in this domain is a fundamental step, as it provides a clear understanding of existing achievements, current limitations, and research gaps that require further investigation. In this context, the most recent and relevant studies directly related to the objectives of this work have been carefully selected, with particular emphasis on indirect solar dryers. Special attention is given to their design configurations, thermal performance, and drying efficiency. The analysis of these studies serves to guide the design choices of the proposed system and to strengthen the scientific relevance of the present work.

II.2. Integration of Thermal Energy Storage Using Phase Change Materials (PCM)

The operation of indirect solar dryers remains strongly dependent on climatic conditions, which makes drying irregular when solar radiation decreases. This constraint limits the effective duration of system use and can affect the quality of the dried product.

In this context, the use of phase change materials represents an effective solution. These materials absorb the excess heat produced during the day and store it in the form of latent energy. When the temperature drops, this stored energy is gradually released, allowing a more stable thermal environment to be maintained.

Thus, the integration of PCM in indirect solar dryers makes it possible to extend the drying duration beyond sunshine hours and to improve the overall thermal performance of the system.

II.2.1. Indirect forced convection dryer with MCP integrated into the sensor

According to Bareen et al. (2024), an indirect forced-convection solar dryer integrated with a phase change material (PCM) was designed (Figure.II.1.**)**, fabricated, and experimentally investigated in order to improve thermal storage and drying continuity. The system comprised a solar energy accumulator (solar air collector with a PCM cavity), a drying chamber, and a blower.

The results showed that after using the PCM, the drying air temperature was maintained between 9 and 12 °C above ambient temperature for approximately 4 hours after sunset. Using the PCM accelerated the process by which Cymbopogon citratus was effectively dried at drying air temperatures between 42 and 59 °C. The daily energy efficiency of the solar energy accumulator reached 35.8%, while the daily exergy efficiency reached 13.84%**.**[5]

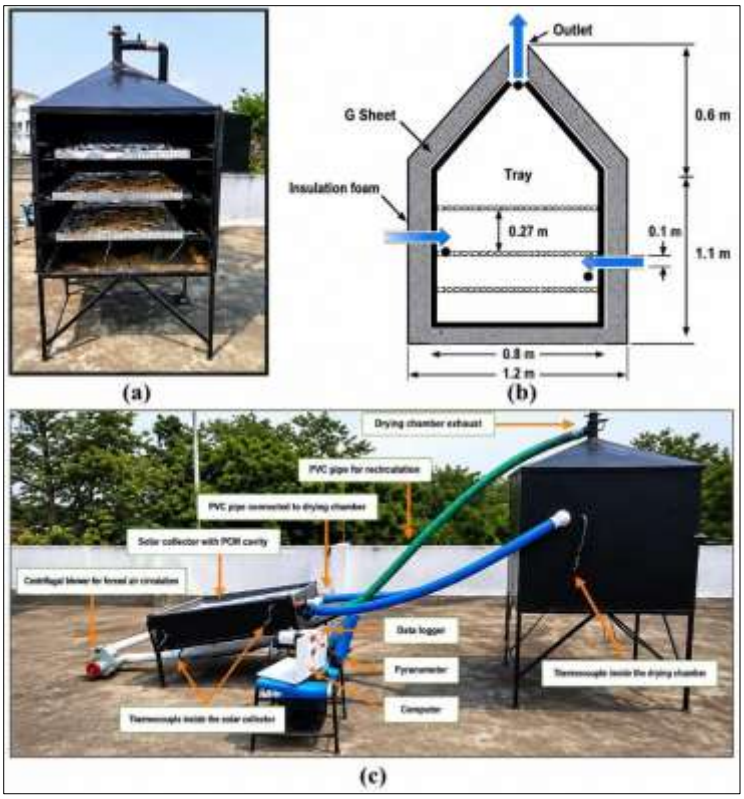


Figure II. 1. Experimental setup: (a) Front view of the drying chamber with tray and dried lemongrass sample, (b) detailed schematic diagram of the drying chamber with the dimensions, (c) image of the whole experimental setup along with all the measuring instruments.

II.2.2. Active indirect dryer with conical MCP and photovoltaic panels

Vijayaregunathan et al. (2025), evaluated an active indirect solar dryer (AMISD) integrating a paraffin-based PCM in a conical configuration (Figure. II. 2.), coupled with PV-powered diverging ducts, for drying Turkey berries in India. PCM integration improved collector efficiency (89.6% vs 35% late afternoon), overall dryer efficiency (15.23% vs 14.8%), and reduced energy consumption (1268 W vs 1384 W). Exergetically, SAC efficiency increased from 6.84% to 7.1% and the sustainability index from 8.01 to 8.1. Economically, the payback period dropped to 0.92 years with PCM versus 1.6 years without, with daily savings doubled [6].

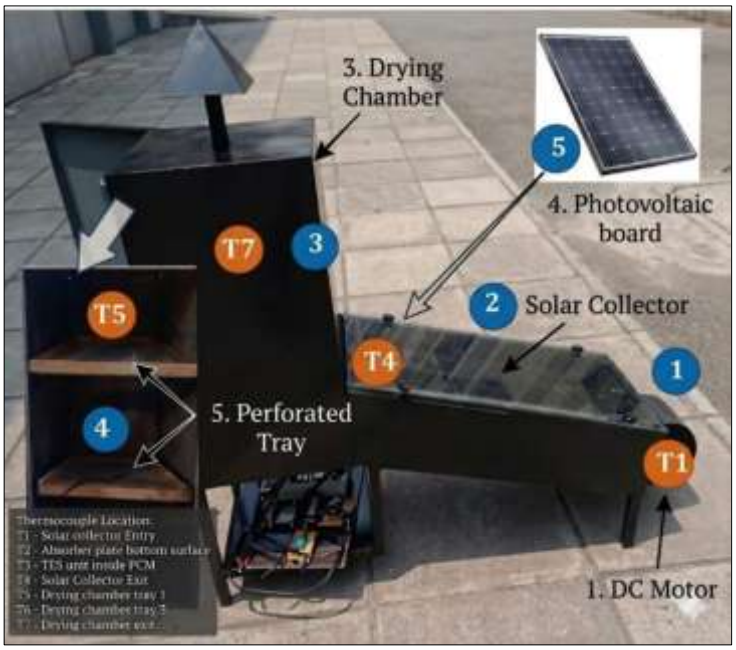


Figure II. 2. Experimental setup.

II.3. Energy, Exergy and Techno-Economic Analyses

A rigorous evaluation of thermodynamic performance is essential for optimizing solar dryers and supporting their large-scale deployment. Energy and exergy analyses make it possible to quantify internal irreversibility, identify sources of energy losses, and compare different dryer configurations and operating modes. These analyses provide valuable insights into system efficiency and contribute to the development of more sustainable, cost-effective, and high-performance solar drying technologies.

II.3.1. Comparison of hybrid dryer, indirect dryer, and shade drying

Yazici and Kose. (2024), present a comprehensive comparative analysis of three drying methods: a novel hybrid dryer, a conventional indirect solar dryer (ISD), and traditional shade drying (Figure. II. 3.). The study integrates energy, exergy, and economic indicators through a 3E analysis. Results confirm the superiority of the hybrid dryer in terms of both energy and exergy efficiencies, while establishing a clear hierarchy among the three approaches. This work represents a useful methodological reference for researchers seeking to position their own drying configurations against existing solutions [7].

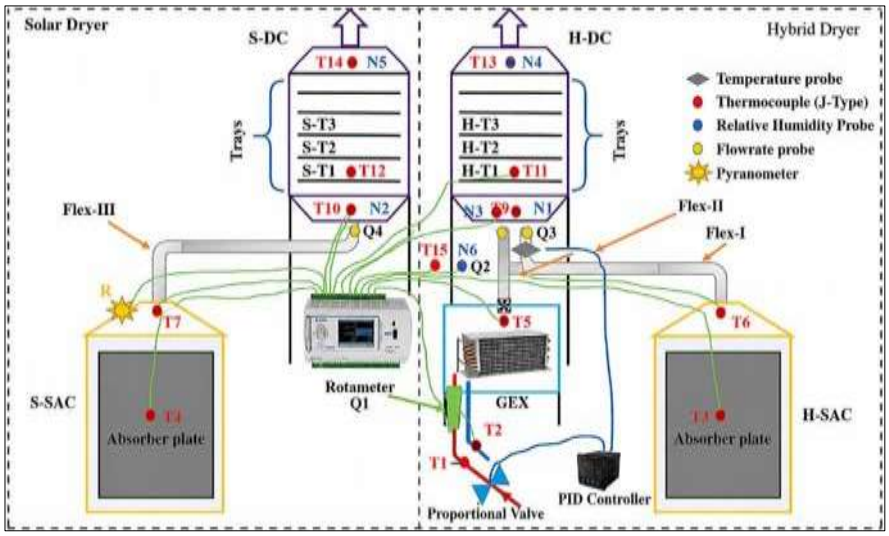


Figure II. 3. Schematic diagram of the experimental setup for a solar dryer and hybrid dryer system with instrumentation and control components.

II.3.2. Energy and exergy analysis of an indirect dryer for oranges

Mawire et al. (2024) experimentally evaluated an indirect forced-convection solar dryer for drying banana slices under four different operating conditions (Figure.II. 4.), combining 16 h and 24 h drying tests with different airflow velocities. The study is distinguished by its detailed instrumentation, including measurements of air velocity inside the drying chamber and thermal profiles across each drying tray. The results showed that the 16 h tests achieved lower final moisture ratios (0.20–0.26) than the 24 h tests (0.28–0.32). Furthermore, despite collector efficiencies varying between 10% and 80%, the average drying efficiency remained comparable across all tests (5.5–6.9%), indicating that airflow rate had only a limited influence on the overall drying performance [8].



Figure II. 4. A photograph of the solar dryer.

II.4. Integration of Smart Technologies (IoT and Artificial Intelligence)

The rapid advancement of the Internet of Things (IoT) and machine learning is opening new opportunities for the real-time monitoring, control, and optimization of solar dryers. This research area is gaining increasing attention in recent scientific literature due to its potential to enhance the efficiency, reliability, and automation of solar drying systems.

II.4.1. Predictive control of an indirect forced convection dryer

Rafiq et al. (2024), propose a modeling and control approach for an indirect forced convection solar dryer based on system identification and Model Predictive Control (MPC) (Figure. II. 5.**)**. Although the modeling aspect is central, the validation relies on experimental data, giving this work an indirect experimental dimension. The MPC approach enables anticipation of solar irradiance variations and real-time adjustment of airflow to maintain optimal drying conditions [9].

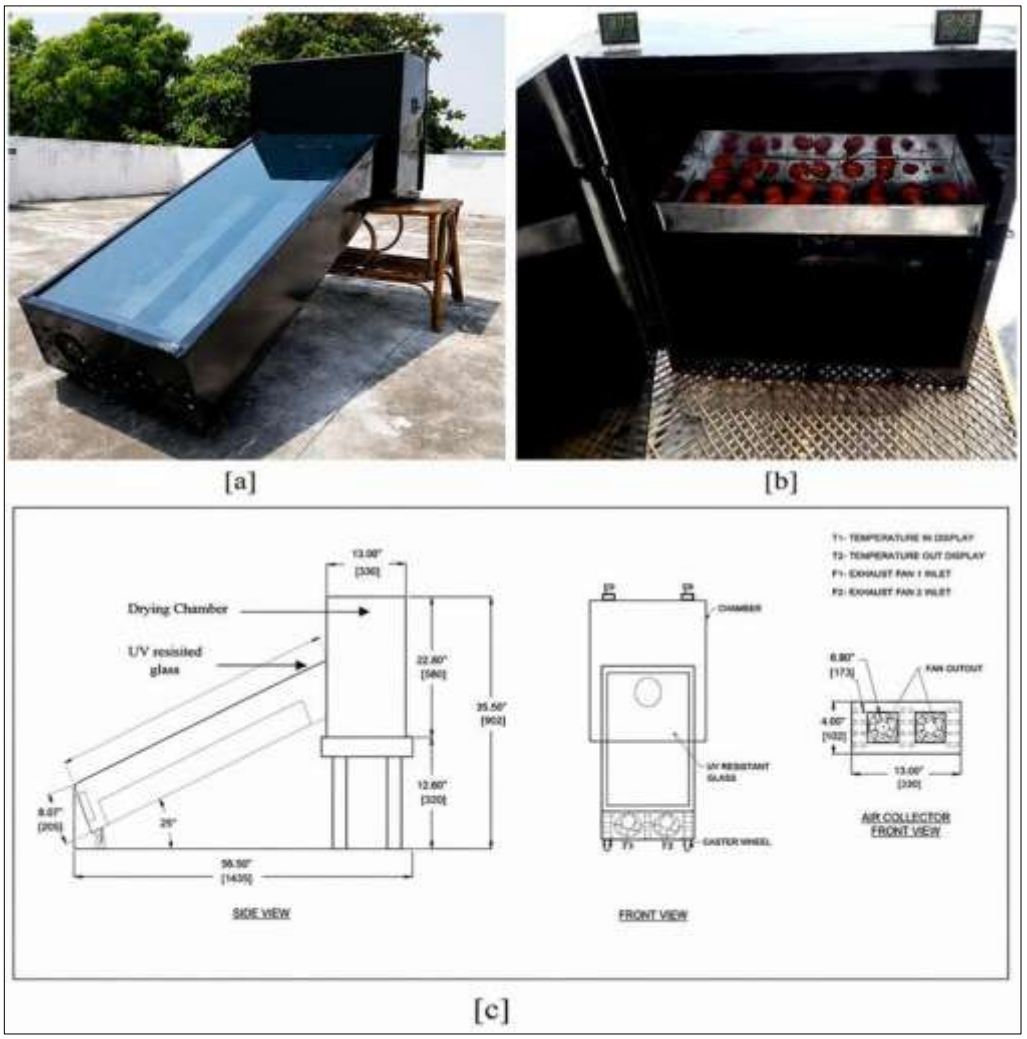


Figure II. 5.Séchoir solaire indirect à convection forcée pour le séchage de tomates cerises.

II.4.2. Connected indirect dryer for temperate crops

Sharma et al. (2025), propose the design of a smart indirect solar dryer integrating IoT technologies to automate and optimize the post-harvest drying process of fruits and vegetables (Figure. II. 6.). The system is distinguished by crop-specific control, allowing the user to set precise temperatures adapted to the product being dried, and ensures real-time monitoring via a cloud platform. Experimental results, obtained under no-load conditions, show an average air velocity of 3.0 m/s, a collector temperature of 57°C, and a stable drying chamber temperature of 45°C, outperforming comparable conventional systems. The authors highlight, however, limitations related to internet connectivity, the technological literacy of rural farmers, and the absence of tests under real loading conditions [10].

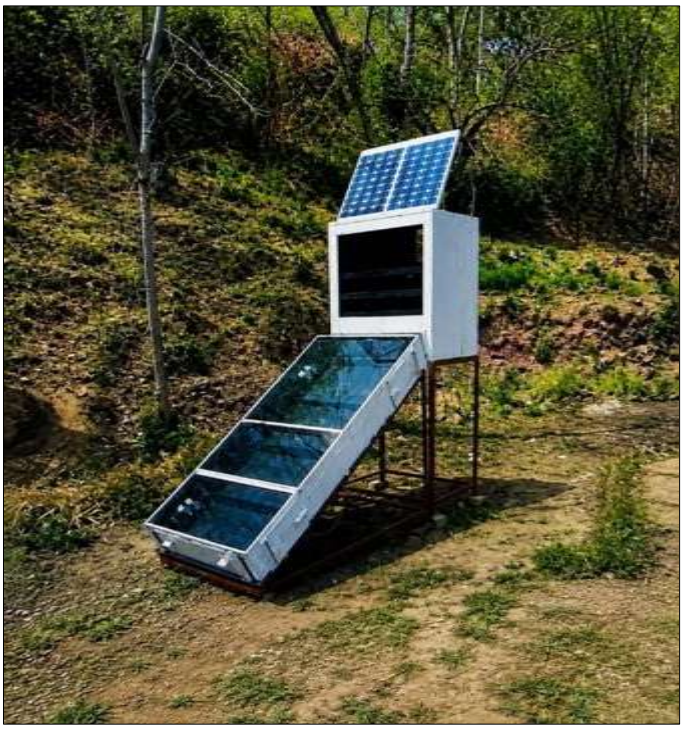


Figure II. 6. Constructed model of the indirect solar dryer for practical use

II.5. Optimization of Structural Configurations and Design Variants

Improving the performance of indirect solar dryers often relies on innovations in the design of the solar collector, drying chamber, and auxiliary systems such as heat exchangers, dehumidifiers, and solar concentrators. These design improvements aim to enhance heat transfer, increase drying efficiency, reduce energy losses, and improve the overall quality of dried products. Several recent studies have explored these approaches, proposing novel configurations and design modifications to optimize the thermal and operational performance of indirect solar drying systems.

II.4.1. Indirect forced convection dryer integrating a silica gel dehumidifier

Zeeshan et al. (2024), propose the design and experimental evaluation of an indirectly forced convection solar dryer integrated with a calcium chloride (CaCl) desiccant (Figure.II. 7.), tested on tomatoes at the NUST University laboratory in Pakistan. The system operates continuously by using solar energy during sunshine hours and the thermally charged desiccant during off-sunshine hours, through DC fans powered by a photovoltaic panel. Results show an overall efficiency of 58.07% and a moisture removal of 56% over two days, significantly outperforming comparable systems reported in the literature (12 to 43%), with a payback

period of 5.14 years and a CO_2 mitigation of 2.0335 kWh/year, thus confirming the potential of this approach for sustainable food preservation in developing countries [11].

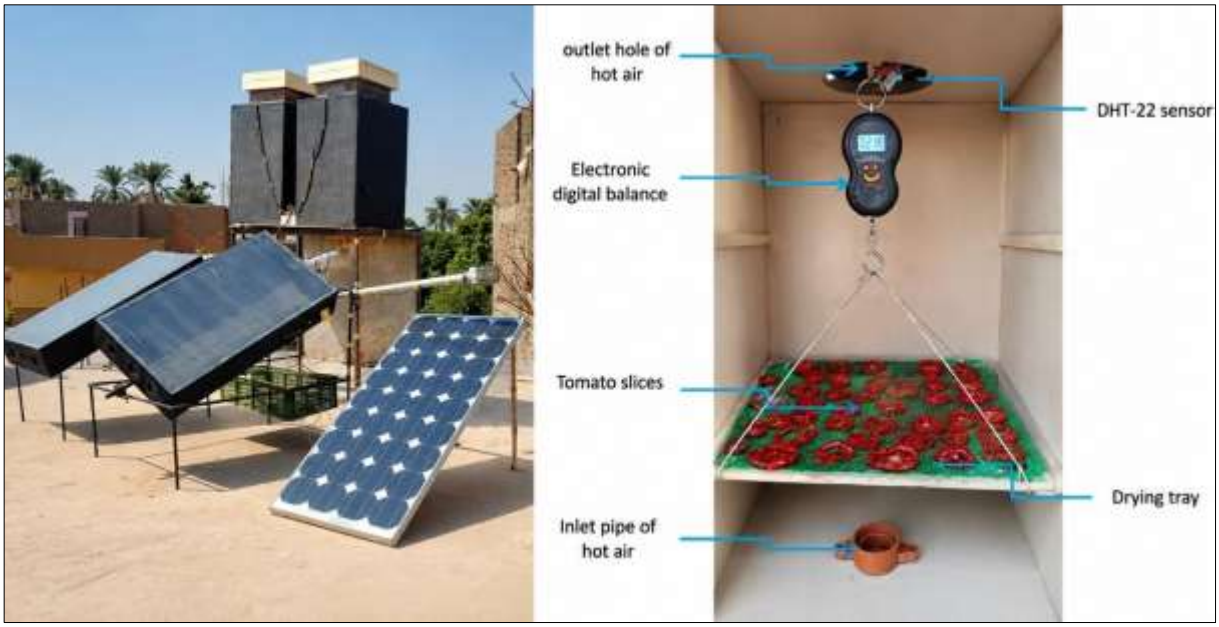


Figure II. 7. Experimental setup of a PV-powered indirect solar dryer: outdoor installation and instrumented drying chamber loaded with tomato slices.

II.4.2. Double-sided absorber indirect solar dryer for vegetables

Hossain et al. (2025), designed, fabricated, and evaluated a photovoltaic-powered indirect solar dryer for vegetable drying in Bangladesh (Figure. II. 8.). The innovative double-sided absorber plate collector was designed to capture solar radiation throughout the day, thereby maximizing solar energy utilization and minimizing heat losses. Experiments were conducted between May and June 2024 using red amaranth, moringa, and coriander leaves. The results showed that the dryer achieved temperatures ranging from 51 to 57 °C and reduced the moisture content of the crops four hours faster than traditional open-sun drying [12].



Figure II. 8. Different parts of solar dryer.

II.6. Drying Kinetics and Product Quality

The ultimate objective of a dryer is to produce a high-quality dried food product within a reasonable time. Therefore, the study of drying kinetics and the physicochemical quality of the final product represents a central research focus in recent studies on indirect solar dryers.

II.6.1. Drying Kinetics and Mathematical Modeling

Touré et al. (2024), conducted an experimental study and thermal modeling of the convective drying of cocoa shells in an indirect solar dryer (Figure. II. 9.). The mathematical modeling, combined with experimental validation, made it possible to identify the most suitable empirical models for describing moisture content decay curves over time [13].



Figure II. 9. The indirect solar dryer used for the drying experiments.

II.6.2. Drying of Apple Slices: Multi-Condition Evaluation

Kaveh et al. (2025), evaluated the performance of different configurations of solar drying chambers and the drying kinetics of apple slices (Figure. II. 10.). Configuration B, improved with a trapezoidal tunnel and solar-powered fans, showed higher efficiency of both the collector (68.74% compared to 56.84%) and the dryer (9.55% compared to 7.5%). Key drying parameters such as activation energy, as well as heat and mass transfer coefficients, were analyzed. The uncertainty estimates confirmed the reliability and accuracy of the obtained results. These findings provide a solid basis for the design and development of pilot-scale solar dryers [14].



Figure II. 10. Experimental setup of a PV-powered indirect solar dryer: (a) full system view with labeled components, (b) close-up of internal fans and drying sample

II.7. Conclusion

The studies presented in this chapter demonstrate that the performance of indirect solar dryers can be enhanced through various approaches, including the integration of phase change materials (PCM), design optimization, smart technologies. In this study, the effect of integrating flexible tubes into the solar collector will be investigate by comparing the system performance with and without tubes.

CHAPTER III
Materials and Methods

Table of contents

III.1. Introduction 28

III.2. Description of the Solar Dryer Prototype 28

III.3. Assembly Components 33

III.4. Assembly of the Drying Chamber and the Solar Collector 35

III.5. Instrumentation and Measuring Instruments 37

III.6. Incorporation of flexible metal pipes into the collector 40

III.7. Experimental Methodology 41

III.8. Conclusion 42

III.1. Introduction

This chapter is dedicated to the description and experimental implementation of an indirect solar dryer developed and tested within the framework of this study. It presents the design configuration of the prototype, the materials used in its construction, and the experimental methodology adopted to evaluate its thermal performance. The experiments were conducted under laboratory conditions. The measurements collected throughout these experiments serve as the basis for the analysis and discussion presented in the following chapter.

III.2. Description of the Solar Dryer Prototype

The objective of this work is to design and build an indirect forced-convection solar dryer primarily intended for drying food products at a small-scale artisanal level. The experimental prototype was constructed in the workshop of the ETAP research laboratory at the University of Tlemcen. This section provides a detailed description of the solar dryer. It covers the general structure, the solar thermal collector, the drying chamber, and the air circulation system to facilitate a better understanding of the device's overall operation.

III.2.1. General Structure of the Dryer

This study presents an experimental investigation of an indirect forced-convection solar dryer incorporating an innovative active-wall concept: the sun-facing wall of the drying chamber, conventionally a thermally inert wooden surface, is replaced by an integrated flat-plate air solar collector. This modification transforms a passive structural element into an active thermal component, allowing the system to recover solar energy that would otherwise be lost through the dryer wall and provide supplementary heating to the air stream before it enters the drying chamber. Two absorber configurations were experimentally compared a conventional flat-plate absorber and a tubular absorber integrating parallel rough-surfaced metallic tubes in order to assess the influence of absorber geometry on the thermal performance of the wall-integrated collector.

The prototype consists of two main components: a solar thermal collector and a drying chamber (figure III.1.a). The solar collector is a vertical flat-plate collector directly integrated and attached to the dryer wall. It is made of wood, glass, and steel, while the drying chamber is constructed from a recycled steel enclosure. This vertical configuration, while promoting compact integration, influences the heat transfer dynamics within the system. The entire system is designed to be simple and cost-effective, using locally available materials.

The operating principle of the solar dryer is based on a forced convective airflow driven by a fan located at the lower part of the drying chamber (figure III.1.b). Ambient air is drawn from the outside through the air inlet and directed into the solar collector. Inside the collector, the air flows over the absorber surface where it gains thermal energy from solar radiation, resulting in an increase in its temperature. The heated air then rises and is guided into the drying chamber, where it passes through the agricultural products to remove moisture through heat and mass transfer processes. Finally, the humid air is expelled to the outside through the outlet, ensuring a continuous airflow through the system and maintaining the drying process efficiency.

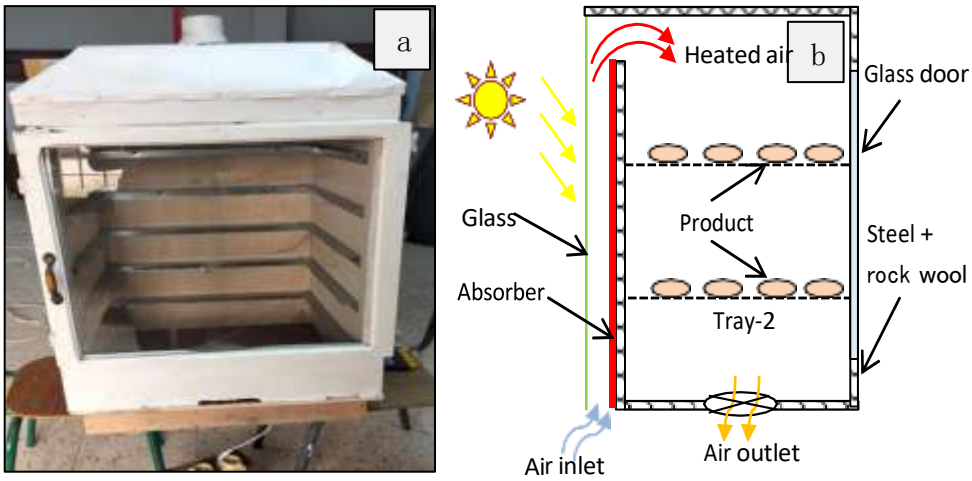


Figure III. 1: (a) The fabricated solar dryer prototype, (b) simplified schematic of the prototype.

III.2.2. Solar simulator

To simulate solar irradiation under controlled laboratory conditions, a solar simulator composed of an array of 28 lamps was used (figure III.2). The system consists of 7 horizontal rows and 4 vertical columns, providing a uniform radiation field over the test surface. Each lamp has a nominal power of 100 W, resulting in a total installed power sufficient to reproduce the thermal effect of solar radiation on the dryer system. The lamps are mounted on a flat plywood support, ensuring a stable and planar irradiation surface. In addition, the simulator is equipped with a mechanical structure that allows adjustment of both height and inclination, enabling variation of the incident radiation angle to better replicate different solar positions. This setup ensures repeatable and controllable experimental conditions for evaluating the thermal performance of the solar dryer.



Figure III. 2: Solar simulator

III.2.3. Solar Thermal Collector

The solar collector used in this system is a vertical flat-plate air heater, similar in concept to conventional solar thermal panels. It has a collection surface area of 0.75 × 0.59 m² and is directly attached to the dryer wall, which promotes a compact system design. The front surface consists of a 5 mm thick transparent glass cover, allowing solar radiation to penetrate into the collector while reducing thermal losses to the surrounding environment. Solar energy is absorbed by an internal absorber plate, made of a metallic sheet coated with matte black paint to maximize solar absorptivity, and is transferred to the air flowing inside the collector, thereby increasing its temperature before it is directed toward the drying chamber. The wooden frame provides additional structural support while contributing to natural thermal insulation, thereby reducing heat losses from the system (figure III.3.a).

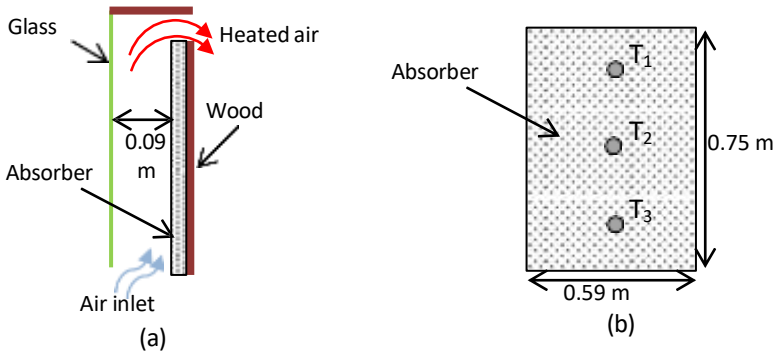


Figure III. 3: Schematic diagram of the solar thermal collector, (a) Side view, (b) front view of absorber. ● Thermocouple positions.

The instrumentation, consisting of three temperature probes (T_1, T_2, T_3), is arranged vertically to cover the critical zones of the absorber according to an exposure gradient to the incident heat flux (figure III.3.b):

T_1 (Top): Located at the upper part of the absorber, it is the closest region to the radiant source and thus receives the highest incident heat flux intensity.

T_2 (Center): Placed at the middle section, it reflects the thermal behavior of the central zone of the absorbing surface.

T_3 (Bottom): Positioned at the lower part, it measures the temperature of the region farthest from the source, where solar irradiation is the lowest.

III.2.4. Drying Chamber

The drying chamber is a recycled steel enclosure with overall dimensions of 0.75 m in height, 0.6 m in length, and 0.48 m in width. To enhance the thermal performance of the dryer and minimize heat losses, the chamber walls are insulated with a layer of rock wool and lined internally with plywood panels. The interior is equipped with metallic mesh trays arranged horizontally at different levels, allowing efficient circulation of hot air through the product layers and ensuring uniform drying (Figure III.4.a).

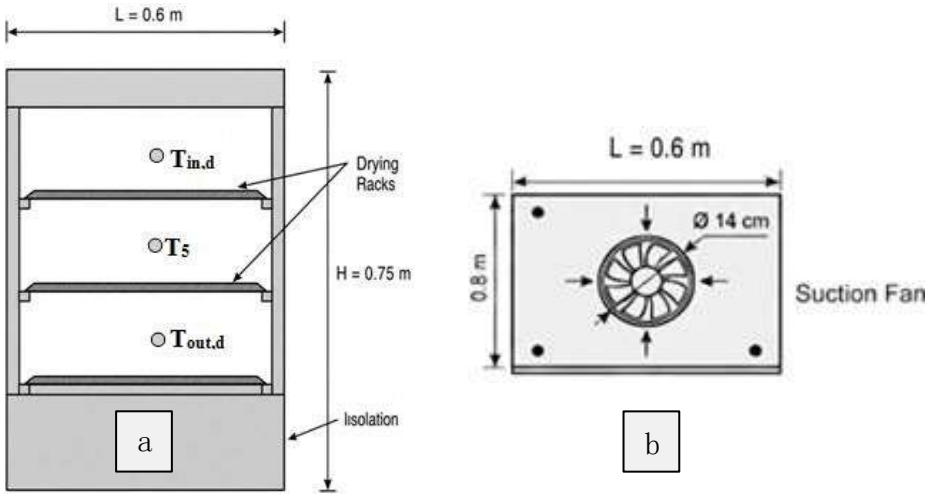


Figure III. 4: Schematic diagram of the drying chamber, (a) Side view, (b) top view. ● Thermocouple positions.

Heated air supplied by the solar collector flows directly through the trays, promoting heat and mass transfer and facilitating the drying of agricultural products. A glass door is

installed at the rear of the chamber, allowing continuous monitoring and inspection of the products during the drying process without disturbing the operating conditions inside the dryer. Air renewal within the chamber is ensured by an exhaust fan mounted at the lower part of the drying chamber (Figure III.4.b). This fan continuously extracts moisture-laden air to the outside, maintaining a favorable drying environment and improving the overall efficiency of the drying process.

To investigate the thermal behavior of the drying chamber and gain a better understanding of the heat transfer mechanisms occurring within it, three thermocouples were installed vertically along the chamber height. The first thermocouple was positioned at the air inlet ($T_{in,\ d}$) to measure the temperature of the air supplied by the solar collector, the second was placed at the mid-height of the chamber (T_5) to monitor the thermal evolution of the airflow, and the third was located at the air outlet ($T_{out,\ d}$) to determine the temperature of the exhausted air. This arrangement enables the characterization of the temperature distribution and thermal gradients within the drying chamber, providing valuable insight into the heat transfer processes and the overall thermal performance of the drying system.

III.2.5. Air Circulation System

Air circulation through the dryer is provided by a 220 W fan OPSSING model installed at the lower part of the drying chamber. The fan has an outlet diameter of 14 cm and is equipped with an adjustable discharge section that can be reduced to smaller diameters. This feature was used to vary the outlet cross-sectional area and, consequently, regulate the airflow rate through the drying system. By modifying the outlet diameter, different airflow conditions could be established, enabling the investigation of their influence on heat and mass transfer processes as well as on the overall drying performance. The adjustable outlet therefore provides a simple and effective means of controlling the operating conditions of the solar dryer during experimental tests.



Figure III. 5: OPSSING electric fan used for forced air circulation.

III.3. Assembly Components

This section presents the different materials and elements used for the fabrication and assembly of the solar dryer prototype. Each element was selected based on its thermal and mechanical properties, as well as its local availability.

- Wood is a natural material characterized by good thermal insulation properties and ease of machining. In this prototype, it is used for the fabrication of the structure and walls of the solar collector, helping to minimize heat losses to the outside.
- Matte black painted metal sheet is a metallic material whose dark surface provides a high capacity for absorbing solar radiation. It constitutes the absorber of the solar collector and plays an essential role in converting solar radiation into thermal energy for air heating.
- Ordinary glass of 5 mm thickness is a transparent material that allows solar radiation to pass through while limiting convective heat losses. It serves as the cover of the solar collector, creating a greenhouse effect that promotes air temperature rise. It is also used for the door of the drying chamber, enabling visual monitoring of the products during the drying process.
- Plywood is a composite wood panel made of several thin bonded layers. It is installed over the rock wool layer on the interior walls of the drying chamber, providing a clean and smooth surface suitable for contact with food products.



Figure III. 6: Matte black painted metal sheet (absorber), plywood panel and glass.

- Rock wool of 7 mm thickness is a mineral-based thermal insulating material, known for its low thermal conductivity and resistance to high temperatures. It is applied to the interior walls of the drying chamber to minimize heat losses and improve the overall thermal performance of the system.
- PROSEAL mastic sealant is a flexible, high-quality sealing product used to fix and seal the glass cover onto the wooden frame of the solar collector. It ensures airtightness and prevents any infiltration of outside air.



Figure III. 7: PROSEAL sealant used for glass cover sealing.

- Screws and fixing elements are metallic components used to assemble the different parts of the prototype, ensuring the mechanical integrity and long-term stability of the overall structure.

III.4. Assembly of the Drying Chamber and the Solar Collector

This section provides a concise overview of the main assembly steps of the solar dryer prototype. It describes the assembly of the solar collector as well as the drying chamber, in order to ensure proper integration between the two elements of the system.

III.4.1. Solar Thermal Collector

The solar thermal collector was entirely fabricated in the laboratory. Its dimensions are: 0.59 m in length, 0.75 m in high, and 0.09 m in thickness.

- The fabrication of the collector followed the steps described below:

1. Assembly of the wooden casing:

The wooden planks were cut to the required dimensions and then assembled into a rectangular casing. This casing forms the outer structure of the collector and provides natural thermal insulation for the walls. The bottom of the casing was left open in order to allow ambient air to enter the collector.

2. Installation of the absorber:

A metal sheet was cut to the inner dimensions of the casing, then placed and fixed at the bottom of it. This sheet constitutes the absorber of the solar collector.

3. Painting of the absorber:

The upper surface of the metal sheet was painted in matte black in order to ensure maximum absorption of solar radiation and to minimize reflection losses.

4. Installation and fixing of the glazing:

An glass pane was cut to the dimensions of the collector and placed on the upper face of the casing. It was fixed using PROSEAL mastic sealant, ensuring good airtightness and holding the glazing firmly in place.



Figure III. 8: Final view of the solar collector.

III.4.2. Drying Chamber

The drying chamber consists of a recovered metallic steel enclosure that was originally designed and constructed as part of a previous research project. For the purposes of the present study, the chamber was reused and modified to meet the specific requirements of the new solar drying system. The modifications introduced in the present work mainly concerned the integration of the new solar collector and the adaptation of the airflow circulation system, enabling the chamber to operate efficiently under the experimental conditions investigated.

III.4.3. General View of the Assembled Prototype

The figure (FigureIII.9) presents a general view of the fully assembled solar dryer prototype, highlighting the integration of the solar thermal collector into the wall of the drying chamber. It also illustrates the relative position of the solar simulator with respect to the solar dryer, showing the experimental arrangement used to reproduce controlled solar irradiation conditions during the tests.



Figure III. 9. Experimental setup in the laboratory: solar simulator facing the solar collector and drying chamber.

III.4.4. Instrumentation and Measuring Instruments

This section presents the different measuring instruments used during the drying experiments. These devices allow the measurement and recording of the physical parameters necessary for monitoring the drying process.

III.4.5. Measurement of Solar Radiation

Solar radiation is a physical quantity that represents the power of solar energy received per unit area. It is measured using a pyranometer, an instrument that converts solar radiation energy into an electrical signal and displays the measured values in digital form. It is oriented in the same direction as the solar collector in order to obtain representative measurements of the radiation received by the system.



Figure III. 10. Solarimeter

III.4.6. Temperature Measurement

Temperature is the most important parameter in the drying process. It is measured using two complementary elements:

Type K thermocouples are temperature sensors consisting of two different metals whose junction generates an electrical voltage proportional to the measured temperature. They allow temperature measurement with high accuracy. In this study, the thermocouples are positioned at the following points:

- At the air inlet of the solar collector.
- At the bottom, middle and top of the absorber.
- At the bottom, middle and top of the drying chamber.
- At the air outlet of the drying chamber.
- Outside for the measurement of ambient temperature.



Figure III. 11: Thermocouples type K

The data logger is an electronic device that collects, stores and displays in real time the temperature values measured by the thermocouples. It ensures continuous and automatic monitoring of temperatures throughout the experiment.



Figure III. 12: Data Logger

III.4.7. Air Velocity Measurement

Air velocity is a physical quantity that represents the displacement of air per unit of time. It is measured using a digital thermo-anemometer 9160SI, an instrument that measures air velocity through an internal propeller and displays the results in several units: m/s, km/h, knots and ft/min. It is positioned at the outlet of the fan in order to measure the air flow rate circulating in the system.



Figure III. 13: Thermo-anemometer

III.4.8. Mass Measurement

Mass is an essential parameter that allows monitoring of the evolution of water loss in the products during drying. It is measured using a digital electronic balance, with an error rate of ± 1 g. Measurements are taken regularly throughout the drying process in order to plot the water loss curve of the products.



Figure III. 14: electronic Balance.

III.5. Incorporation of flexible metal pipes into the collector

In order to enhance the heat transfer between the absorber and the drying air, a modified absorber design was developed. The conventional flat absorber was replaced by an assembly of 6 rough-surfaced aluminum tubes (Figure III. 15. a), each having a length of 0.8 m and a diameter of 9 cm, arranged in parallel within the solar collector. This tube assembly constitutes the new absorber responsible for converting incident solar radiation into thermal energy (Figure III.15.b). The absorber surface was coated with matte black paint to maximize solar energy absorption and minimize radiation reflection losses. The cylindrical geometry of the tubes increases the effective heat transfer area available for convective exchange between the absorber and the airflow, thereby improving thermal energy transfer to the drying air. In addition, the rough surface of the aluminum tubes enhances solar radiation absorption by reducing surface reflectivity, contributing to improved collector thermal performance.



Figure III. 15: (a) flexible metal pipes, (b) integration of pipe into the collector

III.6. Experimental Methodology

The experimental study was conducted in order to analyze the thermal behavior of the solar drying system under different operating conditions. The tests were carried out without product load, with the aim of characterizing solely the thermal performance of the solar collector and the drying chamber, without considering the mass transfer phenomena related to drying.

The experiments were conducted in two distinct phases. The first phase was carried out in the laboratory using an artificial solar simulator, allowing control of the incident radiation. The second phase was performed under outdoor conditions, under real natural solar irradiation, in order to evaluate the operation of the system under representative climatic conditions.

Three levels of solar irradiation were considered: 200, 300, and 400 W/m², combined with three air mass flow rate values: 0.013, 0.015, and 0.017 kg/s. This combination resulted. in a total of nine experimental configurations, each repeated to ensure the reliability and reproducibility of the results.

For each configuration, the test duration was set to one hour, in order to ensure the thermal stability of the system. Temperature measurements were recorded at regular intervals

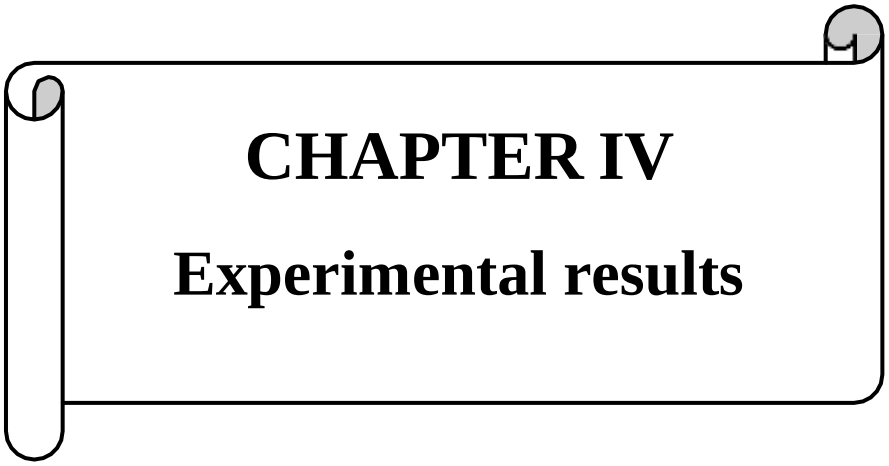
of 5 minutes throughout each experiment, enabling a detailed temporal analysis of the thermal evolution of both the solar collector and the drying chamber.

The results obtained from these experiments will be presented and analyzed in the following chapter.

III.7. Conclusion

The solar drying prototype presented in this chapter represents the result of a design and fabrication work carried out with limited but well-considered means. Every technical choice, from the simplest material to the positioning of the measuring instruments, was motivated by a clear objective: to obtain a functional, economical system adapted to local climatic conditions.

The implementation of this device opens the way to an experimental phase whose results will allow a real evaluation of its thermal performance and overall system efficiency. This is precisely the subject of the following chapter.



CHAPTER IV

Experimental results

Table of Contents

IV.1. Introduction 44
IV.2. Solar Dryer with a Flat-Plate Collector 44
IV.3. Solar Dryer with a metallic tubular absorber 57
IV.4. Summary of key performance indicators for both configurations 63
IV.5. Conclusion 64

IV.1. Introduction

This chapter presents and discusses the experimental results obtained from the performance evaluation of the solar dryer under its two investigated configurations: a conventional flat-plate collector with a smooth absorber and a modified collector incorporating metallic tubes. The primary objective of this analysis is to assess the influence of the collector design on the thermal behavior and overall energy performance of the drying system, and to identify the configuration that provides the most efficient utilization of the available solar energy.

The experimental investigations were carried out under controlled laboratory conditions using a solar simulator. The collected data include measurements of air and absorber temperatures at different locations within the system, airflow rate, and incident solar radiation. Particular attention is given to the effects of operating parameters, such as air mass flow rate and radiation intensity, on the thermal response of both the collector and the drying chamber.

A detailed comparative analysis of the two configurations is performed to highlight the advantages and limitations of each design. The results provide valuable insights into the heat transfer mechanisms governing the system operation and contribute to the identification of the most effective configuration. Furthermore, the findings serve as a basis for proposing design improvements and operational recommendations aimed at enhancing the performance and energy efficiency of solar drying systems for various practical applications.

IV.2. Solar Dryer with a Flat-Plate Collector

This section presents the experimental results obtained for the flat-plate collector configuration, investigated under a constant air mass flow rate of 0.015 kg/s and a constant incident radiation intensity of 330 W/m² without load. Six temperature profiles (T_1, T_2, T_3, $T_{in,d}$, T_5, and $T_{out,d}$) are analyzed to characterize the thermal response of the system during the transient heating period and up to the establishment of a quasi-steady-state regime, which is reached after approximately 60 minutes of operation. The analysis of these temperature evolutions provides valuable insight into the heat transfer processes occurring within both the solar collector and the drying chamber, as well as the thermal behavior of the overall drying system.

IV.2.1. Thermal Behavior Analysis

Figure IV.1 presents the temporal evolution of temperature at six measurement points distributed across the solar collector and the drying chamber. Upon start-up, all temperature profiles exhibit a sharp and rapid rise during the first 20 minutes of operation, reflecting the system's response to the sudden application of the radiative heat flux.

Within the solar collector, T_1 attains the highest temperatures approximately 64°C while T_2 and T_3 stabilize at intermediate values of approximately 43°C and 35°C, respectively. This descending thermal gradient ($T_1 > T_2 > T_3$) is consistent with the vertical arrangement of the thermocouples along the absorber surface and with the geometry of the inclined radiative source.

The three thermocouples are vertically distributed along the absorber: T_1 is located at the top, closest to the radiative source and therefore subjected to the highest incident flux; T_2 is positioned at mid-height, capturing the thermal behavior of the central absorber region; and T_3 is placed at the base, where the incident flux diminishes due to the increasing distance from the source and the inclination geometry.

This configuration directly governs the observed temperature hierarchy. The non-uniform irradiation profile, imposed by the inclination of the radiative source, induces a localized thermal concentration in the upper region of the absorber, which is most pronounced during the early transient phase. As a consequence, the rate of temperature rise at T_1 significantly exceeds that recorded at T3 during the start-up period.

During the transient phase (0–20 min), the temperature rise is markedly faster at T_1 than at T_3, confirming the spatial heterogeneity of the applied heat flux. Furthermore, the integration of the solar collector onto the dryer wall introduces additional thermal inertia into the system: a fraction of the absorbed energy is conducted through the wall during start-up, which moderates the rate of temperature increase of the working fluid relative to what would be expected from an ideally insulated configuration.

Inside the drying chamber, the temperatures $T_{in,d}$, T_5, and $T_{out,d}$ evolve in a nearly identical manner throughout the entire experiment, stabilise close to 27 °C. This quasi-uniform thermal field is attributable to the absence of any hygroscopic load (empty-chamber tests), which eliminates the primary heat sink within the drying space.

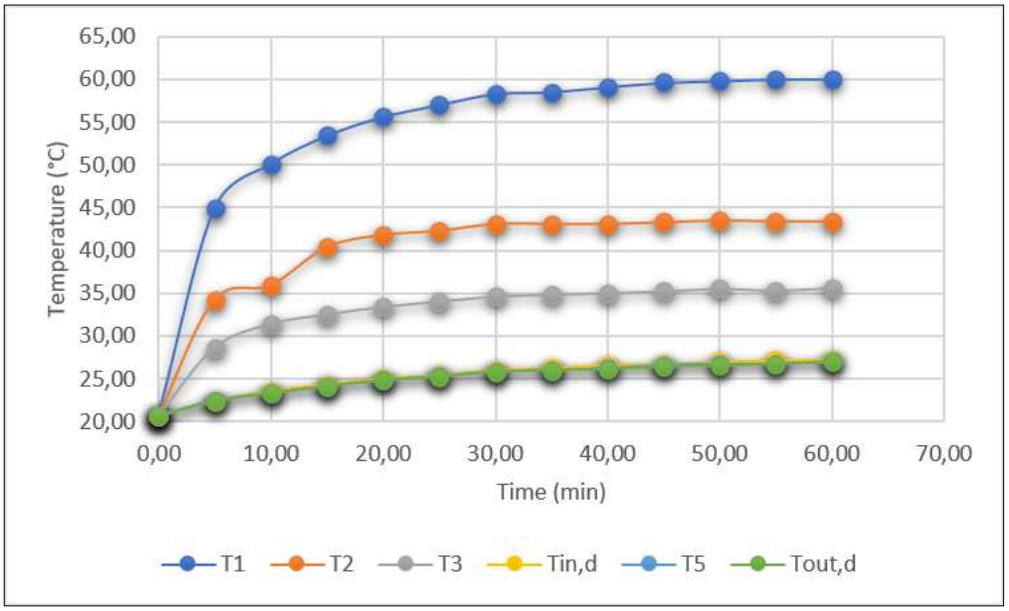


Figure IV. 1: Temporal variation of the temperatures measured in the solar collector (T_1, T_2, and T_3) and the drying chamber ($T_{in,d}$, T_5, and $T_{out,d}$).

Under these conditions, forced air circulation facilitates convective heat extraction from the collector, yet the overall heat transfer to the chamber remains limited. The absence of product also suppresses the latent heat exchange associated with moisture evaporation, which would otherwise be the dominant energy pathway in operational drying conditions. These results thus represent a flat plate thermal characterisation of the system without loading effects.

After approximately 40 minutes of operation, all temperature curves plateau and converge toward a quasi-steady state, indicating the progressive equilibration of the heat transfer processes conduction through the absorber, convection to the working fluid, and conductive losses through the dryer wall. This stabilisation marks the transition from the transient regime to a thermally balanced operating condition.

IV.2.2. Thermal efficiency of the collector

Figure IV.2 illustrates the temporal evolution of the thermal efficiency η of a flat-plate air solar collector over a 60-minute operating period. The curve follows a characteristic monotonically increasing profile, transitioning from a null efficiency at start-up to a near-plateau value of approximately $\eta \simeq 0.68$ at t = 60 min. This behaviour is consistent with the progressive thermal equilibration of the collector under continuous solar irradiation.

During the first 20 minutes, η rises sharply from 0 to approximately 0.30, representing the most dynamic phase of the response. This rapid increase reflects the dominant role of

sensible heat storage within the absorber and the working fluid: as the absorber plate heats up, the temperature difference between the air and the absorber surface grows, intensifying convective heat transfer to the airflow.

At this stage, thermal losses through the glazing and the back insulation remain relatively moderate, as the collector has not yet reached its thermal equilibrium with the environment. The efficiency gain per unit time is therefore at its maximum during this interval.

Between 20 and 40 minutes, η continues to increase but at a progressively decreasing rate, rising from ≈ 0.45 to ≈ 0.62. This deceleration is attributable to the simultaneous growth of convective and radiative thermal losses as the absorber temperature increases. The net useful heat gain transferred to the air consequently grows more slowly, causing the efficiency curve to flatten.

This phase also reflects the growing influence of thermal inertia in the collector-dryer wall assembly, which continues to absorb a fraction of the incident energy without contributing directly to the air heating process.

After approximately 40 minutes, the efficiency curve approaches a quasi-plateau, with η stabilising between 0.63 and 0.68. This stabilisation indicates that the system has reached a near-steady energy balance: the useful heat extracted by the airflow equals the difference between the absorbed solar flux and the total thermal losses.

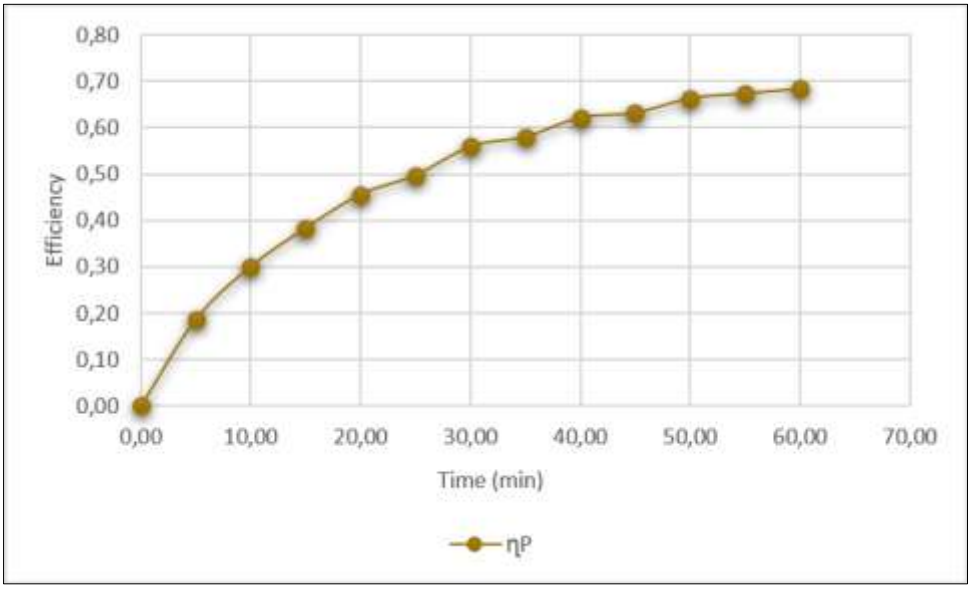


Figure IV. 2: Temporal evolution of thermal efficiency of the collector.

The residual slight increase observed between t = 50 and t = 60 min may be attributed to the progressive reduction of the thermal inertia effect as the collector wall approaches its steady-state temperature, allowing a marginally greater fraction of the absorbed flux to be transferred to the working fluid.

IV.2.3. Effect of flow rate variation at constant irradiance (I = 330 W/m²)

This section presents a comparative analysis of the experimental results obtained under three distinct air mass flow rates :0.012 kg/s, 0.015 kg/s, and 0.017 kg/s at a constant radiation of 330 W/m². The objective is to assess the influence of flow rate variation on the thermal behavior of the flat-plate air solar collector under identical radiative conditions. Three key parameters are examined and compared across the tested configurations: the absorber temperature T_2, which reflects the mean(moyen) thermal state of the absorber surface and its response to varying convective cooling intensities; the temperature difference between the collector inlet and outlet ($\Delta T = T_{in,d} - T_{amb}$), which serves as a direct indicator of the heat gain transferred to the working fluid; and the thermal efficiency η of the collector, which quantifies the fraction of the incident solar energy effectively converted into useful heat. This multi-parameter comparison aims to identify the optimal operating flow rate that maximise heat extraction while maintaining acceptable absorber temperatures.

A. Absorber temperature

Figure IV.3 illustrates the temporal evolution of the absorber temperature T_2 recorded under three distinct air mass flow rates: 0.012 kg/s, 0.015 kg/s, and 0.017 kg/s at a constant solar irradiance of 330 W/m².

It is observed that all three temperature profiles exhibit a similar transient behaviour: a rapid rise during the first 20 minutes of operation, followed by a progressive stabilisation toward a quasi-steady state after approximately 40 minutes. At quasi-steady state, T2 reaches approximately 50 °C at 0.012 kg/s, 44 °C at 0.015 kg/s, and 45 °C at 0.017 kg/s.

The reduction in T_2 observed when the flow rate increases from 0.012 kg/s to 0.015 kg/s (a decrease of approximately 6°C) is consistent with the enhancement of forced convective heat transfer between the absorber surface and the working fluid. A higher mass flow rate increases the convective heat transfer coefficient, thereby intensifying heat extraction from the absorber plate and limiting thermal accumulation within it.

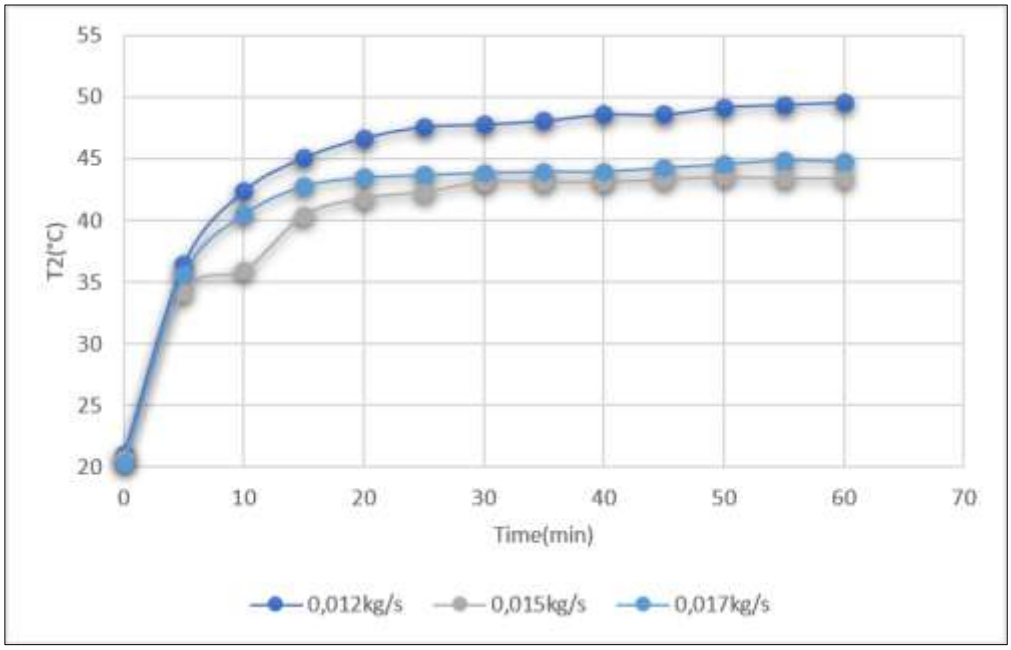


Figure IV. 3: Effect of air mass flow rate on the temporal evolution of the collector temperature T_2.

However, a further increase in flow rate from 0.015 kg/s to 0.017 kg/s results in a slight rise in T_2, from approximately 44 °C to 45 °C. At such elevated flow rates, two competing effects come into play: the convective heat transfer coefficient *h* continues to increase which tends to cool the absorber plate more effectively yet the capacity of the air to absorb heat over the full length of the collector diminishes, as the contact time between the air and the absorber surface becomes too short for sufficient thermal equilibration to occur. The slight rise in T_2 at 0.017 kg/s suggests that this second effect begins to dominate, indicating that a mass flow rate of 0.015 kg/s represents a near optimal local operating condition for absorber cooling under the tested irradiance of I = 330 W/m², offering the best compromise between convective transfer intensity and adequate air residence time within the collector channel.

B. Solar collector heat gain of ($T_{in,d} - T_{amb}$)

Figure IV.4 presents the temporal evolution of the temperature difference between the drying chamber inlet and the ambient ($\Delta T = T_{in,d} - T_{amb}$) for the three tested mass flow rates: 0.012 kg/s, 0.015 kg/s, and 0.017 kg/s, under a constant solar irradiance of 330 W/m². This temperature difference serves as a direct indicator of the thermal elevation imparted to the air by the collector.

All three profiles exhibit a consistent transient behaviour, characterised by a steep increase during the first 20 minutes followed by a gradual stabilisation toward a quasi-steady state beyond 40 minutes. At quasi-steady state, ΔT for 0.012 kg/s reaches approximately 6.4**°C**, ΔT for 0.015 kg/s attains the highest value of approximately 6.6°C, while ΔT for 0.017 kg/s stabilises at a lower value of approximately 5.8 °C.

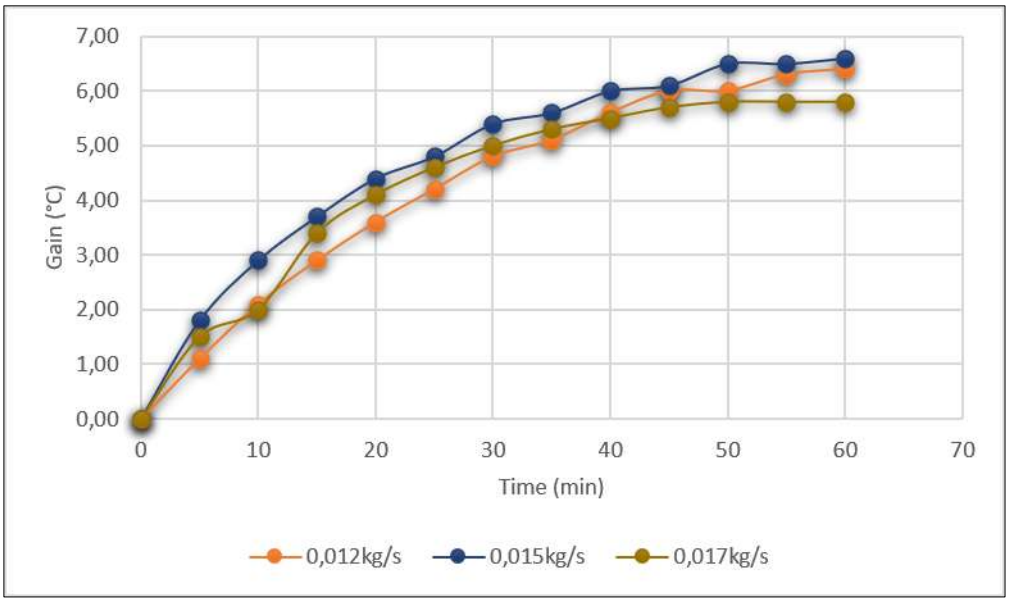


Figure IV. 4: Variation of the collector thermal gain with time at different mass flow rates.

This hierarchy directly reflects the influence of the air residence time within the collector channel. At 0.012 kg/s, the air travels slowly through the collector, allowing moderate thermal equilibration with the absorber surface. Increasing the flow rate to 0.015 kg/s slightly improves the convective exchange conditions, resulting in a marginal increase in ΔT. However, a further increase to 0.017 kg/s reduces the residence time to the point where the air exits the collector before reaching sufficient thermal equilibration with the absorber surface, leading to a lower temperature rise despite the higher flow velocity. These results confirm that 0.015 kg/s represents the near-optimal flow rate for maximising the air temperature elevation at the collector outlet under the tested irradiance of 330 W/m².

C. Thermal efficiency of the solar collector

Figure IV.5 illustrates the variation of the thermal efficiency η of the flat-plate air solar collector as a function of the air mass flow rate, at a constant solar irradiance of 330 W/m². The curve reveals a non-monotonic behaviour with a clear efficiency peak at the intermediate flow rate. At 0.012 kg/s, η reaches approximately 53%, which represents the lowest recorded efficiency among the three tested conditions. This relatively modest value, despite the slow flow allowing long contact time, suggests that the dominant limiting factor at

this flow rate is the weak convective exchange between the absorber and the air.

As the flow rate increases to 0.015 kg/s, η rises significantly to approximately 68%, representing an absolute gain of +15% relative to the lowest flow rate. This sharp improvement indicates that the transition toward a more turbulent flow regime substantially enhances the convective heat transfer coefficient, allowing the air to extract heat from the absorber far more effectively. The efficiency peak at this point suggests that the system operates under the most favorable combination of heat transfer intensity and thermal contact duration.

When the flow rate is further increased to 0.017 kg/s, η decreases slightly to approximately 66.5%. The magnitude of this drop roughly 1.5 % is relatively small but physically significant, as it marks the onset of a regime where the gain in convective coefficient no longer compensates for the reduction in the air temperature rise caused by the shorter transit time through the collector. The curve's asymmetry is also noteworthy: the rise from 0.012 to 0.015 kg/s is steep (+15%), whereas the decline from 0.015 to 0.017 kg/s is gradual (−1.5%), suggesting that the system is more sensitive to insufficient flow than to excessive flow within this range.

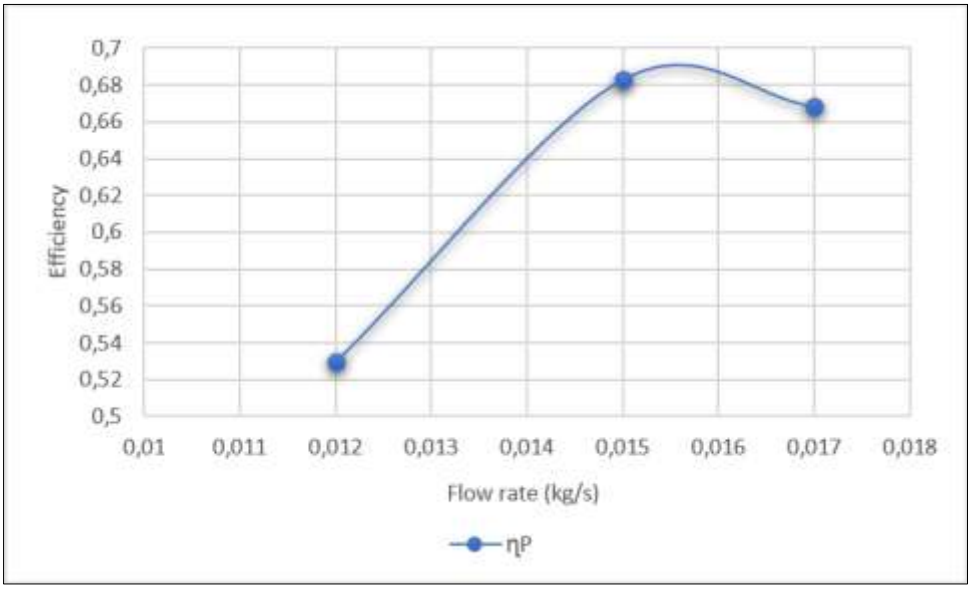


Figure IV. 5: Effect of air mass flow rate on the thermal efficiency of the flat-plate solar collector (ηL).

Overall, these results identify 0.015 kg/s as the optimal operating flow rate under the tested irradiance, and suggest that further increases beyond this value would yiel progressively diminishing returns in thermal performance.

IV.2.4. Effect of irradiance variation at constant flow rate (ṁ = 0.015 kg/s)

- **Absorber temperature**

This section examines the influence of the incident irradiance intensity on the thermal behavior of the solar dryer. The experimental tests were conducted under three distinct irradiance levels: 204 W/m², 330 W/m², and 414 W/m² produced by a solar simulator, while maintaining a constant air mass flow rate of ṁ = 0.015 kg/s throughout all trials. Flow rate of ṁ = 0.015 kg/s was retained as the reference operating condition for this entire series of tests, as it was previously identified as the optimal flow rate for this collector configuration to ensure that the system operates at its best convective performance level, allowing the effect of irradiance variation to be assessed under the most thermally favourable airflow conditions.

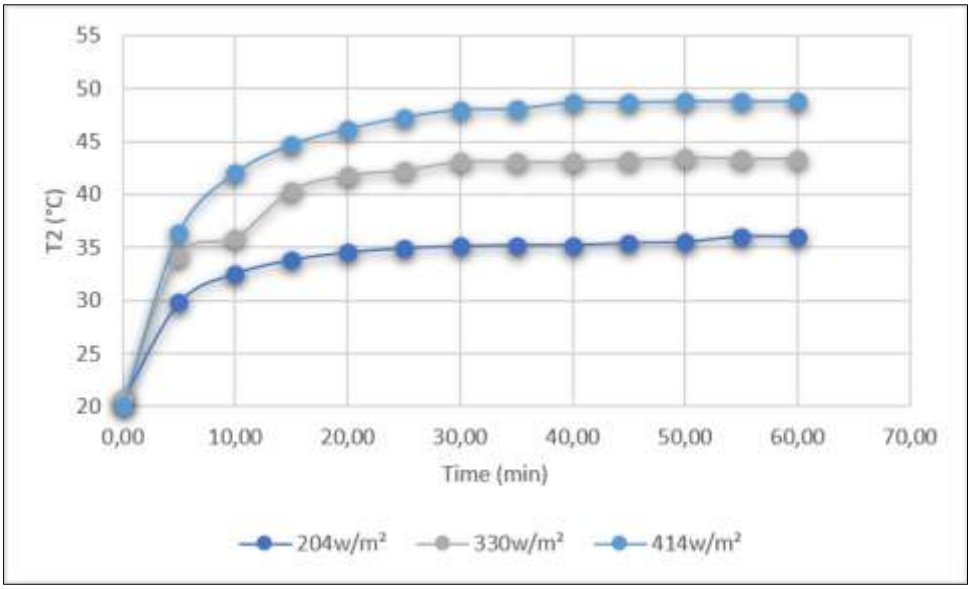


Figure IV. 6: Effect of solar irradiance on the temporal evolution of the collector temperature T_2.

Figure IV.6 presents the temporal evolution of the absorber temperature T_2 under three irradiance levels: 204 W/m², 330 W/m², and 414 W/m² at a constant mass flow rate of $\dot{m}$=0.015 kg/s. All profiles follow a consistent transient pattern: a steep temperature rise during the first 20 minutes of operation, followed by a progressive stabilisation toward a quasi-steady state beyond 40 minutes.

A clear and monotonic increase with irradiance is observed. At quasi-steady state, T_2 reaches approximately 36 °C at 204 W/m², 44 °C at 330 W/m², and 49 °C at 414 W/m², representing successive gains of approximately +8 °C and +5 °C respectively. This direct relationship between irradiance and absorber temperature follows directly from the energy conservation principle applied to the absorber: a higher incident radiative flux delivers a greater amount of energy per unit area to the absorber surface, increasing the net heat absorbed. Since the mass flow rate and the convective conditions are held constant across all three tests, the additional energy input cannot be fully extracted by the airflow, resulting in a higher equilibrium temperature of the absorber plate.

- **Solar collector heat gain ($T_{in,d} - T_{amb}$)**

Figure IV.7 presents the temporal evolution of the temperature difference between the drying chamber inlet and the ambient ($\Delta T = T_{in,d} - T_{amb}$) under three irradiance levels: 204 W/m² (ΔT_1), 330 W/m²(ΔT_2), and 414 W/m²(ΔT_3), at a constant mass flow rate of $\dot{m}$ = 0.015 kg/s.

All three profiles follow a consistent transient pattern: a progressive increase during the first 30 minutes of operation, followed by a gradual stabilisation toward a quasi-steady state beyond 40 minutes. However, the magnitude of the thermal gain differs significantly between the three irradiance levels, revealing a strong sensitivity of the air temperature elevation to the incident radiative flux. An increase in irradiance leads directly and consistently to an increase in the thermal gain of the collector.

At quasi-steady state, ΔT_1 stabilises at approximately 3.5°C, ΔT_2 reaches approximately 6.5 °C, and ΔT_3 attains the highest value of approximately 7.0 °C. The most notable observation is the substantial jump between 204 W/m² and 330 W/m². An increase of approximately +3.0 °C in thermal gain compared to the more modest increment of +0.5 °C recorded between 330 W/m² and 414 W/m². This progressive deceleration in thermal gain growth suggests that the system exhibits a diminishing sensitivity to irradiance increases at higher flux levels.

At low irradiance (204 W/m²), the energy delivered to the absorber is limited, resulting

in a modest temperature elevation of the working fluid. As irradiance increases to 330 W/m², the additional radiative input is effectively converted into sensible heat of the airflow, producing a significant gain in ΔT. However, at 414 W/m², although the absorber receives a greater flux which increases radiative heat losses to the surroundings and limits the efficiency of heat transfer to the working fluid.

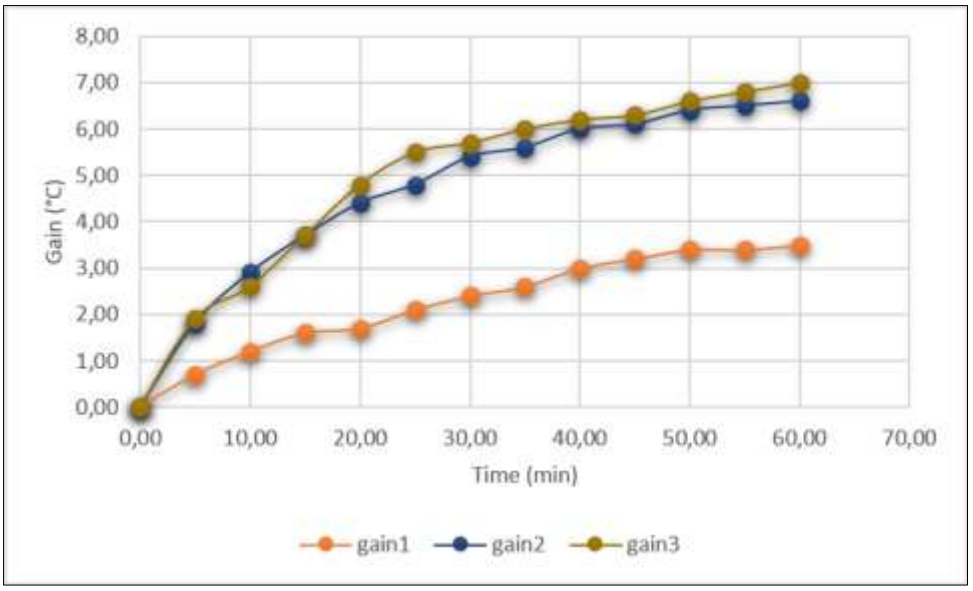


Figure IV. 7:Temporal evolution of the collector thermal gain under different solar irradiance levels

These results show that the thermal gain of the collector increases with irradiance, but not proportionally. At low irradiance levels, any increase in flux produces a notable improvement in the air temperature rise. At higher irradiance levels, however, the benefit of additional flux becomes more limited, since a growing fraction of the absorbed energy is lost to the surroundings rather than transferred to the working fluid.

- **Thermal efficiency of the solar collector**

Figure IV.8 presents the evolution of the thermal efficiency η of the flat-plate air solar collector as a function of the incident irradiance intensity, at a constant mass flow rate of ṁ = 0.015 kg/s. The curve reveals a bell-shaped behavior, characterized by the existence of a well-defined efficiency peak at the intermediate irradiance level.

At the lowest tested irradiance of 204 W/m², the thermal efficiency reaches approximately 60%. At this flux level, the system is strongly dependent on thermal losses relative to the captured flux: the available radiative energy is insufficient to overcome the thermal resistances of the collector effectively, and a disproportionate fraction of the absorbed energy is consumed in compensating for conductive, convective, and radiative losses rather than being transferred to the working fluid. As a result, the efficiency remains limited despite

the relatively low absorber temperature.

As the irradiance increases to 330 W/m², the thermal efficiency rises to its maximum value of approximately 68%. At this operating point, the incident flux is sufficient to ensure efficient heat transfer to the airflow, while the absorber temperature remains moderate enough that radiative losses which scale with the fourth power of the absorber surface temperature (T_2^4) do not yet become dominant. This irradiance level therefore represents the optimal operating condition for this collector configuration, offering the most favourable balance between energy input, heat transfer intensity, and thermal loss magnitude.

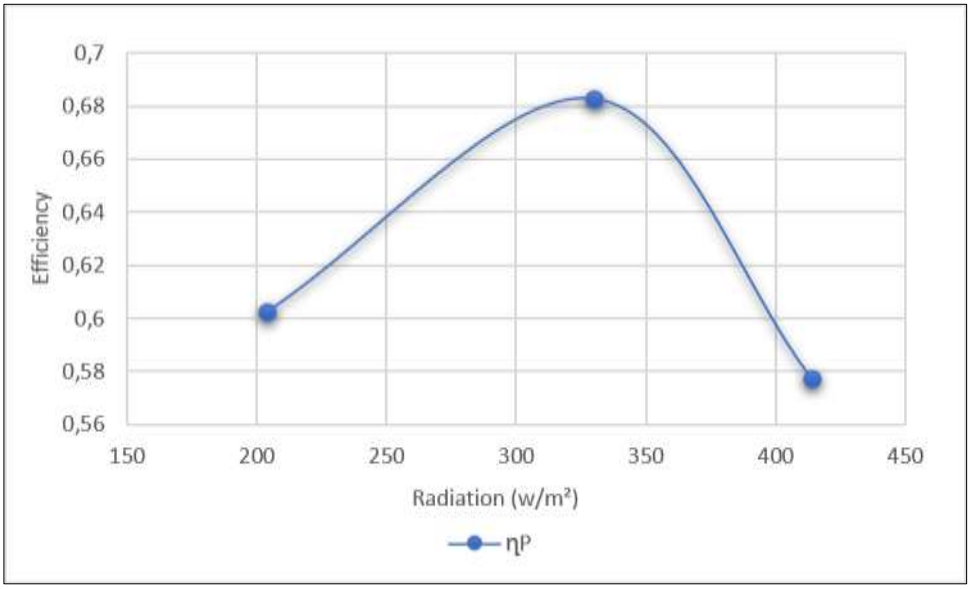


Figure IV. 8: Variation of the thermal efficiency (η_L) as a function of solar irradiance.

A further increase in irradiance to 414 W/m² results in a significant drop in thermal efficiency, falling to approximately 58% the lowest recorded value among the three tested conditions. Beyond the optimal threshold, the overheating of the absorber plate leads to substantial thermal losses, both through the dryer wall by conduction and to the surroundings by radiative emission. Since the flat plate configuration lacks an internal tube, it does not possess a sufficiently enhanced heat extraction mechanism to evacuate this excess thermal energy rapidly enough to maintain a high efficiency. Consequently, the growing losses outpace the gain in absorbed energy, and the net fraction of incident flux converted into useful heat decreases markedly. The drop of approximately 10**%** between 330 and 414 W/m² underlines the strong sensitivity of the system to thermal losses at high irradiance levels.

These results demonstrate that the thermal efficiency of the collector exhibits an optimal irradiance range around 330 W/m² under the tested operating conditions, and that operating significantly above this threshold leads to a deterioration in thermal performance driven by the accelerated growth of absorber heat losses.

The analysis of the results obtained with the flat plate collector highlights its limitations in adapting to varying operating conditions. Despite increases in either the air mass flow rate or the incident irradiance intensity, the improvement in thermal performance remains limited, and the efficiency tends to plateau below a satisfactory level. This behaviour reflects an incomplete exploitation of the available radiative energy, primarily attributable to a non-uniform heat distribution across the absorber surface and insufficiently optimised thermal exchange between the absorber plate and the circulating air.

In order to address these limitations, a new collector configuration has been proposed, consisting of replacing the conventional flat-plate absorber with an array of integrated metallic tubes. This structural modification aims to increase the effective heat exchange surface area, improve the uniformity of heat distribution across the absorber, and enhance the energy transfer between the absorber and the drying airflow. The objective is thereby to achieve a more complete valorisation of the incident radiative energy and superior thermal performance across a broader range of operating conditions, independently of the specific flow rate or irradiance level applied to the system.

IV.1. Solar Dryer with a metallic tubular absorber

In order to enhance the convective heat transfer between the absorber and the drying airflow, a modified absorber design was developed and integrated into the solar collector. The conventional flat-plate absorber was replaced by an assembly of 6 rough-surfaced aluminium tubes. The outer surface of the aluminium tubes was coated with matte black paint, chosen for its high solar absorptivity and low reflectivity, in order to maximise the absorption of incident radiation and minimise optical losses. The cylindrical geometry of the tubes offers two distinct advantages over the conventional flat-plate design: first, it significantly increases the effective heat exchange area available for convective interaction between the absorber surface and the circulating air; second, the curved surface geometry promotes a more uniform distribution of the absorbed heat flux along the collector length, reducing localised overheating. Furthermore, the intentionally rough surface texture of the aluminium tubes serves a dual purpose: it enhances solar radiation absorption by further reducing surface reflectivity, and it promotes local flow turbulence in the vicinity of the tube walls, which intensifies the convective heat transfer coefficient and improves the overall thermal energy transfer to the drying air.

IV.1.1. Comparative Thermal Performance Analysis of a Flat-Plate Absorber and an Absorber with Tubes

A. Absorber temperature

For comparison of the absorber temperatures between the two configurations, the flat plate absorber tested at I = 330 W/m² and the tubular absorber tested at I = 320 W/m² under a constant mass flow rate of $\dot{m}$ = 0.015 kg/s is presented in table IV.1.

Table IV. 1: A comparison of the absorber temperatures between the two configurations

Collector	Flat plate	With tubes
T_1	64°C	58°C
T_2	43°C	42°C
T_3	35°C	32°C

The results reveals two significant and complementary improvements introduced by the tubular absorber design:

- A general reduction in absorber temperatures is observed across all three measurement points. T_1 decreases from 64 °C to 58 °C (−6°C), T_2 from 43 °C to 42 °C (−1°C), and T_3 from 35 °C to 32 °C (−3 °C). This overall reduction in absorber temperature is a direct indicator of enhanced heat transfer between the absorber surface and the working fluid: the metallic tubes increase the effective contact area between the absorber and the circulating air, intensifying convective heat extraction and preventing excessive thermal accumulation within the absorber plate. In other words, the heat absorbed from the incident radiation is more efficiently and rapidly transferred to the drying airflow, rather than being stored in the absorber material or dissipated as thermal losses.
- The temperature gap between the three measurement points is noticeably reduced in the tubular configuration. In the flat plate case, the difference between T_1 and T_3 reaches 29 °C (64 − 35 °C), whereas in the tubular configuration this gap narrows to only 26 **°C** (58 − 32 °C). This reduction in the longitudinal thermal gradient along the absorber surface indicates a more uniform heat distribution within the tubular absorber. The cylindrical geometry of the tubes, combined with their rough surface texture, promotes a more homogeneous convective exchange along the entire length of the collector, attenuating the localised thermal concentration that was predominantly observed at T_1 in the flat plate configuration. A more uniform temperature distribution is particularly beneficial for drying applications, as it ensures a more consistent thermal environment within the collector and reduces the risk of localised overheating that could otherwise accelerate thermal losses.

B. Thermal efficiency

Figure IV.9 presents a direct comparison of the temporal evolution of the thermal efficiency η between flat plate configuration (η_L, I = 330 W/m²) and the tubular absorber configuration (η_T, I = 320 W/m²), both tested at a constant mass flow rate of $\dot{m}$ = 0.015 kg/s.

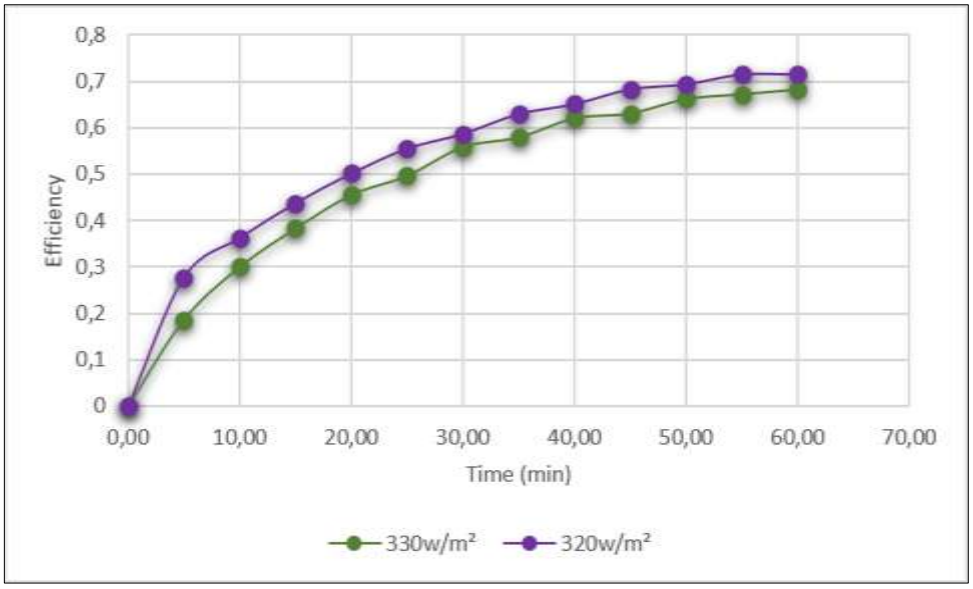


Figure IV. 9: Comparison of the thermal efficiency of the smooth flat-plate collector and the tubular absorber collector.

The tubular absorber configuration consistently exhibits higher efficiency values throughout the entire duration of the experiment, with the gap between the two curves being visible from the very early stages of operation and maintained until quasi-steady state is reached. At quasi-steady state, the flat plate configuration stabilises at approximately **68%**, while the tubular absorber configuration attains approximately **72%** representing an absolute improvement of + 4 %. This result is particularly noteworthy given that the tubular absorber was tested under a marginally lower irradiance (320 W/m² versus 330 W/m²), meaning that the observed efficiency gain is achieved despite a slightly less favourable energy input. Had both configurations been tested under strictly identical irradiance conditions, the improvement attributable to the tubular design would likely be even more pronounced.

The integration of parallel metallic tubes onto the absorber surface constitutes an effective and measurable thermal enhancement strategy, yielding a 4% improvement in thermal efficiency under comparable operating conditions, and confirming the superiority of the tubular absorber design over the conventional flat-plate configuration for this solar dryer application.

C. Effect of radiations

Figures IV.10 presents the thermal efficiency η of the flat-plate collector (η_L) and the tubular absorber collector (η_T) as a function of the incident irradiance, at a constant mass flow rate of $\dot{m}$ = 0.015 kg/s.

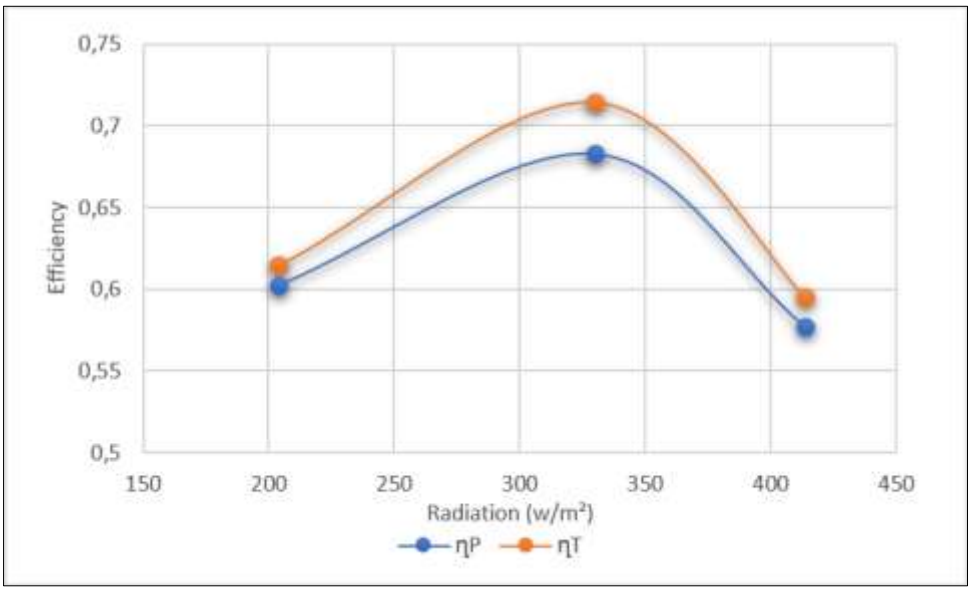


Figure IV. 10: Variation of collector thermal efficiency with air mass flow rate for the two absorber configurations.

A direct comparison between the two configurations reveals a consistent and systematic improvement in thermal efficiency across all tested irradiance levels when the tubular absorber is used.

The most significant improvement is observed at the optimal irradiance of 330 W/m², where the tubular configuration reaches a peak efficiency of approximately 72%, compared to 68% for the flat plate an absolute gain of +4%. This improvement is directly attributable to the enhanced convective heat transfer facilitated by the metallic tubes.

These results demonstrate that the tubular absorber configuration consistently outperforms the flat-plate design across the entire tested irradiance range, with the most meaningful improvement occurring at moderate irradiance levels where the enhanced convective exchange has the greatest impact on the energy balance of the collector. The integration of metallic tubes onto the absorber surface therefore constitutes a thermally effective design modification, particularly well-suited for operating conditions in the low-to-moderate irradiance range.

D. Effect of mass flow rate

Figures IV.11 present the thermal efficiency η of the flat-plate collector as a function

of the air mass flow rate, at a constant irradiance of I = 330 W/m². The comparison between the two curves reveals not only a quantitative improvement in efficiency, but also a fundamentally different behavioural response to flow rate variation between the two configurations.

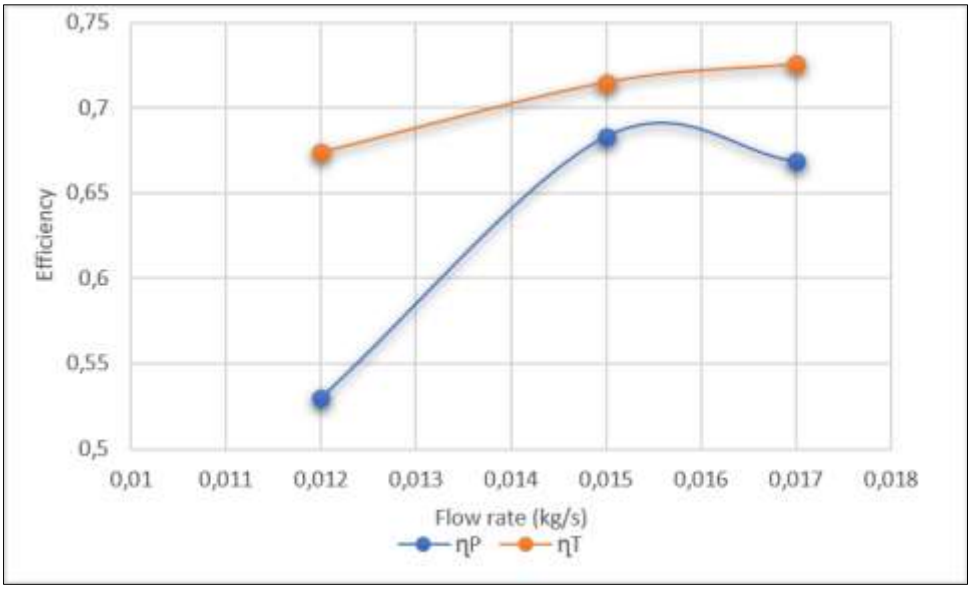


Figure IV. 11: Variation of collector thermal efficiency with solar irradiance for the two absorber configurations

In the flat plate configuration, the efficiency exhibits a bell-shaped behaviour: it rises from 53% at 0.012 kg/s to a peak of 68% at 0.015 kg/s, before declining to 66.5% at 0.017 kg/s. As discussed previously, this non-monotonic behaviour reflects the competing effects of convective enhancement and reduced air residence time, with 0.015 kg/s representing the optimal operating point for the flat-plate absorber.

In sharp contrast, the tubular absorber configuration (η_T) exhibits a continuously increasing efficiency across the entire tested flow rate range: η rises steadily from 67.5% at 0.012 kg/s to 71.5% at 0.015 kg/s, and continues to increase to 72.5% at 0.017 kg/s, with no sign of decline. This fundamentally different behaviour indicates that the tubular absorber is capable of sustaining and even improving its thermal performance at higher flow rates, without suffering from the residence time limitation that constrains the flat plate configuration. The enhanced air-absorber contact area provided by the metallic tubes ensures that even at higher flow velocities, sufficient heat transfer occurs between the absorber surface and the working fluid, compensating for the shorter transit time and maintaining a high thermal efficiency.

From a quantitative standpoint, the most remarkable improvement is observed at the lowest flow rate of 0.012 kg/s, where the tubular configuration achieves 67.5% compared to

only 53% for the flat plate an absolute gain of +14.5%. This substantial difference highlights the critical role of the tubes at low flow rates: in the flat plate case, the weakly turbulent flow regime severely limits convective heat transfer, whereas the rough surface texture and cylindrical geometry of the tubes promote sufficient local turbulence to maintain efficient heat extraction even at low velocities. At 0.015 kg/s, the gain narrows to +3.5 **%** (71.5% vs. 68%), as the flat plate configuration approaches its own optimal operating condition. At 0.017 kg/s, the gain widens again to +6 **%** (72.5% vs. 66.5%), confirming that the tubular configuration handles higher flow rates more effectively than the flat-plate design.

These results demonstrate that the integration of metallic tubes onto the absorber surface not only improves the absolute thermal efficiency of the collector, but also broadens its optimal operating range: while the flat plate configuration is confined to a narrow optimal flow rate window around 0.015 kg/s, the tubular absorber maintains high and increasing efficiency across the entire tested range, making it a more robust and adaptable design for variable operating conditions.

IV.2. Summary of key performance indicators for both configurations

Table IV. 2: Summary of key performance indicators for both configurations

Parameter	Condition	Flat-plate	Tubular	Δ
ABSORBER TEMPERATURES: I = 330/320 W/m², ṁ = 0.015 kg/s				
T_1 (top of absorber)	Quasi-steady state	64 °C	58 °C	**−6 °C**
T_2 (centre of absorber)	Quasi-steady state	43 °C	42 °C	**−1 °C**
T_3 (bottom of absorber)	Quasi-steady state	35 °C	32 °C	**−3 °C**
Longitudinal gradient T_1–T_3	Quasi-steady state	29 °C	26 °C	**−3 °C**
THERMAL EFFICIENCY : Effect of flow rate (I = 330 W/m²)				
η at 0.012 kg/s	Quasi-steady state	53%	67.5%	**+14.5%**
η at 0.015 kg/s	Quasi-steady state	68%	71.5%	**+3.5%**
η at 0.017 kg/s	Quasi-steady state	66.5%	72.5%	**+6%**
THERMAL EFFICIENCY : Effect of irradiance (ṁ = 0.015 kg/s)				
η at 204 W/m²	Quasi-steady state	60%	62%	**+2%**
η at 330 W/m² (optimal)	Quasi-steady state	68%	72%	**+4%**
η at 414 W/m²	Quasi-steady state	58%	59%	**+1%**
BEHAVIOURAL RESPONSE				
η vs. flow rate curve shape	—	Bell-shaped	Monotonically increasing	—
Optimal flow rate	—	0.015 kg/s	> 0.017 kg/s	—
Optimal irradiance	—	330 W/m²	~320 W/m²	—

Table IV.2 provides a consolidated summary of the key thermal performance indicators recorded for both the flat-plate and tubular absorber configurations under all tested

operating conditions. The values presented correspond to quasi-steady state measurements and cover three main aspects: the absorber temperature distribution, the influence of mass flow rate on thermal efficiency, and the influence of irradiance intensity on thermal efficiency. This table facilitates a direct and systematic comparison between the two configurations, highlighting the improvements brought by the tubular absorber design in terms of heat extraction efficiency, temperature uniformity, and operational flexibility.

IV.3. Conclusion

The experimental investigation conducted in this chapter has provided a comprehensive comparative characterisation of two air solar collector configurations a flat plate design without internal enhancement and a modified design integrating an array of parallel metallic tubes under varying mass flow rates and irradiance levels. The key findings of this study can be summarised as follows:

1) Flat plate configuration:

- The collector achieved a maximum thermal efficiency of 68% under optimal conditions ($\dot{m}$ = 0.015 kg/s, I = 330 W/m²), with a well-defined optimal flow rate at 0.015 kg/s beyond which efficiency begins to decline.
- The thermal efficiency exhibited a bell-shaped response to both flow rate and irradiance variations, reflecting the narrow optimal operating window of the flat-plate design.
- At low flow rates (0.012 kg/s), efficiency dropped significantly to 53%, due to the weakly turbulent flow regime and the dominant boundary layer thermal resistance.
- At high irradiance levels (414 W/m²), efficiency fell to **58%**, driven by the disproportionate growth of thermal losses from the overheated absorber surface.

2) Tubular absorber configuration:

- Absorber temperatures were systematically reduced across all measurement points: T_1 decreased by −6 °C, T_2 by −1 °C, and T_3 by −3 °C, confirming enhanced convective heat extraction from the absorber surface.
- The longitudinal thermal gradient along the absorber was reduced from 29 °C to 26 °C, indicating a more uniform heat distribution along the collector length.

- The thermal efficiency was improved across the entire tested irradiance range, with a peak efficiency of **72%** at 330 W/m² a gain of +4 % over the flat plate.
- Unlike the flat plate configuration, the tubular absorber exhibited a continuously increasing efficiency with flow rate, reaching 72.5% at 0.017 kg/s, demonstrating a broader and more robust optimal operating range.
- The most significant improvement was recorded at the lowest flow rate of 0.012 kg/s, where the tubular configuration achieved 67.5% compared to only 53% for the flat plate an absolute gain of +14.5 %.

3) Overall conclusion:

These results confirm that the integration of parallel metallic tubes onto the absorber surface constitutes a meaningful and effective thermal enhancement strategy, simultaneously improving heat extraction efficiency, temperature uniformity, and operational flexibility across a wide range of flow rate and irradiance conditions. The tubular absorber configuration is therefore validated as a superior design for solar drying applications compared to the conventional flat-plate absorber.

CHAPTER V

Results and Discussion

Table of Contents

V.1. Introduction 67
V.2. Description of the complete solar drying system 67
V.3. Measuring Devices and Instruments 69
V.4. Organization of Experimental Tests 69
V.5. Experimental Results 70
V.6. Thermal behaviour analysis of the solar dryer 71
V.7. Evolution of Product Mass 75
V.8. Product after drying 77
V.1. Conclusion 78

V.1. Introduction

The laboratory tests carried out using a solar simulator constituted an essential first step in evaluating the performance of the solar dryer. In order to complement and validate these results, a real-condition experiment was conducted outdoors, under natural sunlight.

This chapter is dedicated to the presentation of this experimental campaign carried out over three days. The drying of two agricultural products, namely banana and mint, was studied. The results obtained are analyzed and compared with those from the laboratory tests, with the aim of globally assessing the performance of the developed solar dryer.

V.2. Description of the complete solar drying system

This section presents the outdoor experimental campaign conducted at the University of Tlemcen (latitude 34.9°N, longitude 1.3°W) during the month of June (18th, and 22nd June), under real solar irradiance conditions. The complete solar drying system was assembled by coupling the primary flat-plate air solar collector previously fabricated and independently characterised with the active-wall drying chamber, via a flexible metallic duct ensuring the continuity of the airflow between the two components. The entire system was oriented southward to maximise the collection of incident solar radiation throughout the day (figure V.I).



Figure V. 1: General view of the solar dryer installed under real conditions

The airflow pathway within the system follows a serial thermal circuit: the ambient air is first drawn through the primary solar collector, where it undergoes an initial stage of thermal elevation through convective heat exchange with the main absorber surface. The pre-heated air is then directed through the flexible metallic duct into the wall-integrated secondary collector the active wall where it undergoes a second stage of supplementary heating before entering the drying chamber. Inside the chamber, the hot air flows over the drying trays, extracting moisture from the agricultural products through convective mass transfer. The humid air is subsequently evacuated to the outside through the outlet orifice, with the airflow throughout the entire circuit being maintained by a mechanical fan ensuring forced convection conditions.

The outdoor experimental campaign was organised into three successive tests. The first experiment was conducted without any drying load, using the flat-plate absorber configuration, in order to establish a thermal baseline characterisation of the complete coupled system under real solar conditions and to assess its thermal behaviour in the absence of any hygroscopic product. The second and third experiments introduced two agricultural products banana slices and mint leaves into the drying chamber, tested successively with the flat-plate absorber and the tubular absorber configuration. The banana was cut into thin slices of approximately 3 mm thickness, with a constant initial mass of 208 g maintained across both trials. The mint was arranged in the form of whole leaves, with an initial mass of 63 g. In parallel with the second experiment, a witness drying tray was placed in the open air under identical solar exposure, serving as a reference for direct comparison between the performance of the solar dryer and conventional open-air sun drying (figure V.2).



Figure V. 2: Banana slices and mint leaves arranged on the trays before drying

The third experiment reproduced the same drying protocol using the tubular absorber configuration, allowing a direct assessment of the thermal and drying performance improvement achieved by the enhanced absorber design under real operating conditions.

V.3. Measuring Devices and Instruments

The physical quantities monitored during this experimentation are solar radiation, temperatures at various points of the dryer, and the mass of the products being dried.

- Incident solar radiation was measured using a pyranometer.
- Temperatures were recorded using six thermocouples connected to a data acquisition system (datalogger), enabling automatic data recording every 30 minutes. The thermocouples were positioned at the following locations:
  - Collector 1: at the middle of absorber ($T_{p,c1}$), and air outlet of collector ($T_{out,c1}$) ;
  - Collector 2 (improved wall): at the middle of absorber ($T_{p,c2}$), at the air inlet ($T_{in,\,c2}$) and air outlet ($T_{out,c2}$).
  - Drying chamber: at outlet of the chamber ($T_{out,ch}$).
- The glazing temperature (T_g) was measured punctually using an infrared thermometer, allowing a non-contact surface measurement.
- The ambient temperature was measured using weather station.
- The mass of the products was measured using a balance, with readings taken every hour. At each weighing, the trays were removed from the dryer, placed on the balance, and then returned to their initial position.

V.4. Organization of Experimental Tests

The tests were organized over two distinct days, each fulfilling a specific objective.

- **Day 1 : June 18, 2026 (drying without tubes)**

The first test took place from 09:15 to 16:09, without tubes in the collector. Banana and mint trays were placed inside the drying chamber. In parallel, two reference trays one of banana and one of mint were placed in the open air in order to compare indirect solar drying with natural air drying.

- **Day 2 : June 22, 2026 (drying with tubes)**

The second test took place from 09:15 to 17:25, with tubes integrated into the collector. The same products were placed exclusively inside the dryer. This day aimed to evaluate the impact of adding tubes on the thermal performance of the collectors (C_1 and C_2) and, consequently, on the efficiency of the drying process.

V.5. Experimental Results

The results obtained during the three experimental days are presented in this section in the form of commented graphs. Each measured quantity is analyzed in order to identify the observed trends and to evaluate the performance of the solar dryer under real conditions.

V.5.1. Climatic Conditions

Before analyzing the thermal performance of the dryer chamber, it is necessary to characterize the climatic conditions that prevailed during each test day. in our study, solar radiation incident on the collector 2 (improved wall) and ambient temperature are indeed the main input parameters that determine the behavior of the drying chamber.

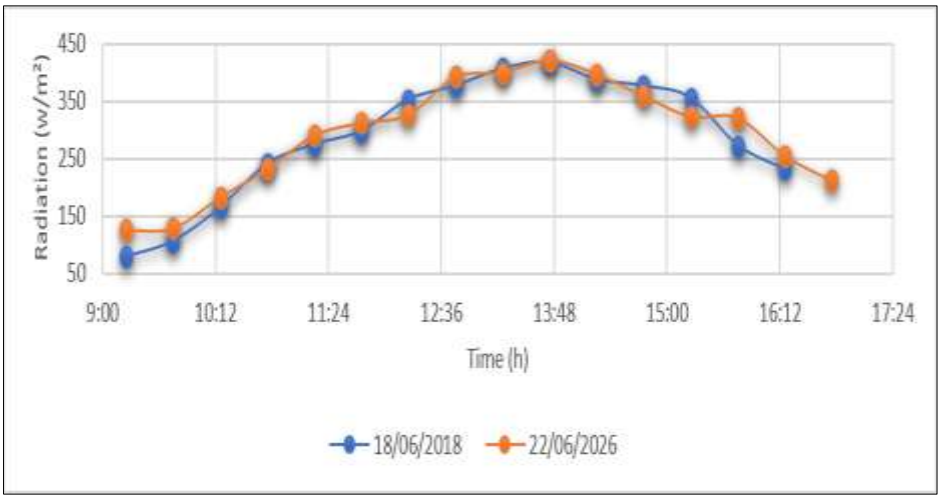


Figure V. 3: Evolution of solar radiation during the two Experiments

The figure V.3 illustrates the evolution of incident solar radiation (W/m²) as a function of time (minutes) for the two experimental days. The curves present a bell-shaped profile characteristic of the daily solar radiation cycle, marked by a progressive increase in the early morning, a maximum reached around midday, followed by a gradual decrease in the late afternoon.

The irradiance levels recorded on the 18th and 22nd June are broadly comparable, ranging from approximately 80–120 W/m² at the start of measurements to peak values between 410 and 420 W/m² around solar noon. The highest peak irradiance was recorded on 22nd June (420 W/m²), followed closely by 18th June (410 W/m²). Both profiles exhibit a smooth and well-defined bell-shaped diurnal curve, indicative of clear sky conditions with minimal cloud interference throughout the measurement period. These two days therefore provide the most representative and comparable dataset for assessing the thermal and drying performance of the solar dryer under stable natural solar irradiance conditions.

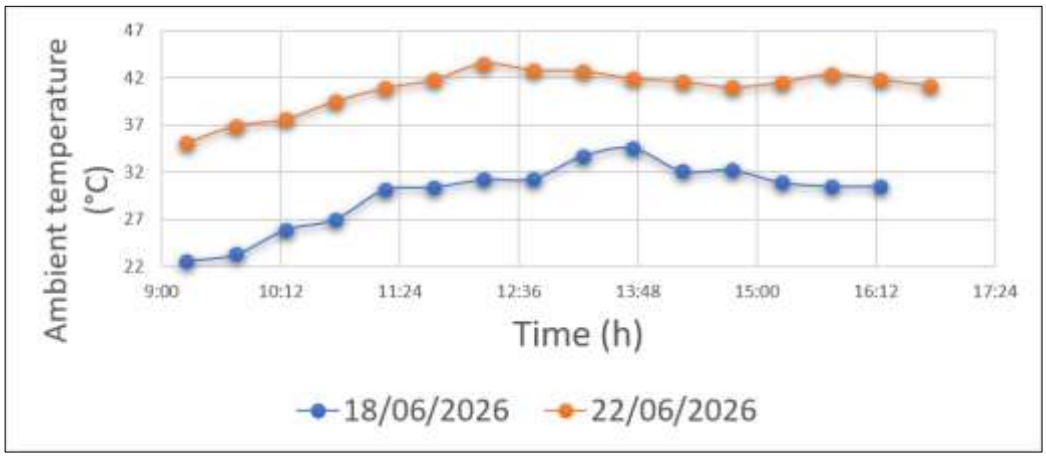


Figure V. 4: Evolution of ambient temperature during the two experiments

The figure above represents the evolution of ambient temperature (°C) as a function of time (minutes) for the three experimental days. It can be observed that June 22 records the highest ambient temperatures, ranging between 35°C and 44°C, while June 17 and 18 present more moderate temperatures, varying approximately between 22°C and 34°C.

This rise in ambient temperature on June 22 is directly linked to the higher solar radiation intensity observed on that day. Higher outdoor temperatures promote heat exchange at the dryer level and contribute to the increase in internal temperatures of the system.

V.6. Thermal behavior analysis of the solar dryer

The analysis of temperatures recorded at various points of the dryer allows the thermal behavior of the system and the efficiency of heat transfer between the solar collector and the drying chamber to be evaluated. The results of June 18 and June 22 are presented separately in order to highlight the effect of adding tubes to the collector**.**

V.6.1. Solar dryer without tubes (day 1)

The figure V.5 represents the evolution of temperatures (°C) at various points of the dryer as a function of time (minutes) during the day of June 18. All curves present a bell-shaped profile, consistent with the evolution of solar radiation throughout the day.

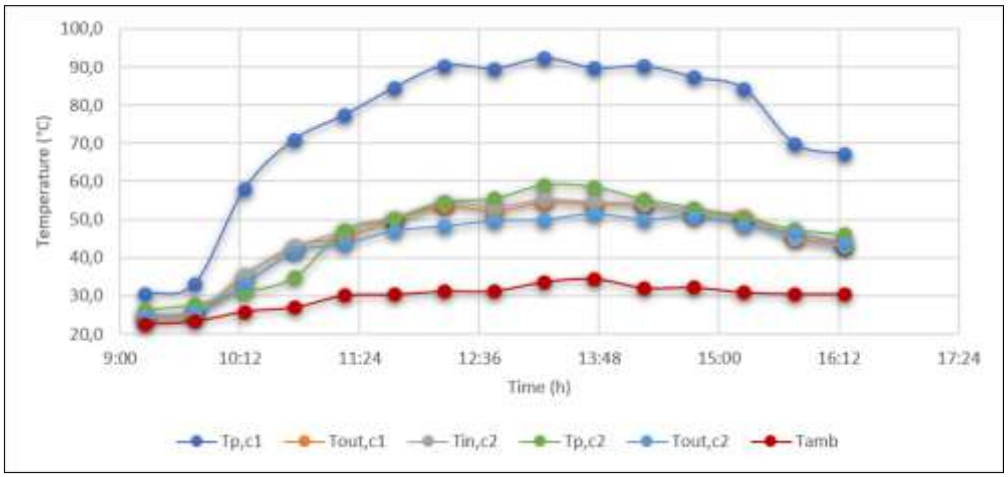


Figure V. 5: Temporal evolution of the temperature of the different components of the solar dryer without tubes

- Regarding the primary collector (C_1), the absorber temperature $T_{p,c1}$ reaches remarkably high values, attaining a peak of approximately 93 °C around solar noon, while the air outlet temperature $T_{out,c1}$ stabilises at approximately 55 °C**.** The substantial temperature difference between the absorber and the outlet air (35°C) reflects the thermal resistance between the absorber plate and the working fluid, indicating that a significant fraction of the absorbed solar energy is stored within the absorber plate or dissipated as thermal losses rather than being fully transferred to the airflow. Nevertheless, $T_{out,c1}$ represents a considerable thermal elevation of approximately 25 °C above the ambient temperature, confirming the effective heat transfer capability of the primary collector under outdoor conditions.
- Regarding the wall-integrated secondary collector (C_2)**,** a more nuanced behaviour is observed. The air enters C_2 already pre-heated at approximately 55 °C (equal to $T_{out,c1}$) and the absorber temperature $T_{p,c2}$ reaches approximately 60 °C, which is only marginally higher than the inlet air temperature. Consequently, the temperature driving force available for heat transfer within C_2 is significantly reduced compared to C_1. More importantly, the air outlet temperature of C_2 ($T_{out,c2}$ = 52 °C) is found to be slightly lower than its inlet temperature ($T_{out,c1}$ = 55 °C), indicating a cooling of the air as it passes through C_2. This result reveals that, despite the absorber of C_2 being warmer than the incoming air, the thermal losses through the glazing and the active wall envelope exceed the supplementary heat gain provided by the C_2 absorber**,** resulting in a negative thermal balance for the secondary collector under these conditions. This finding highlights a critical limitation of the current system assembly.
- A circuit inversion is proposed as a corrective design modification. In the revised configuration, the ambient air would enter the system first through C_2, where it

undergoes an initial pre-heating stage, and then pass through the primary collector C_1, where it receives the main and more intense thermal elevation before being introduced into the drying chamber.

V.6.2. Solar dryer with tubes (day 2)

The figure V.6 represents the evolution of temperatures (°C) at various points of the dryer with tubes as a function of time (minutes) during the day of June 22. The curves present the same bell-shaped profile as the previous day, however with generally higher values.

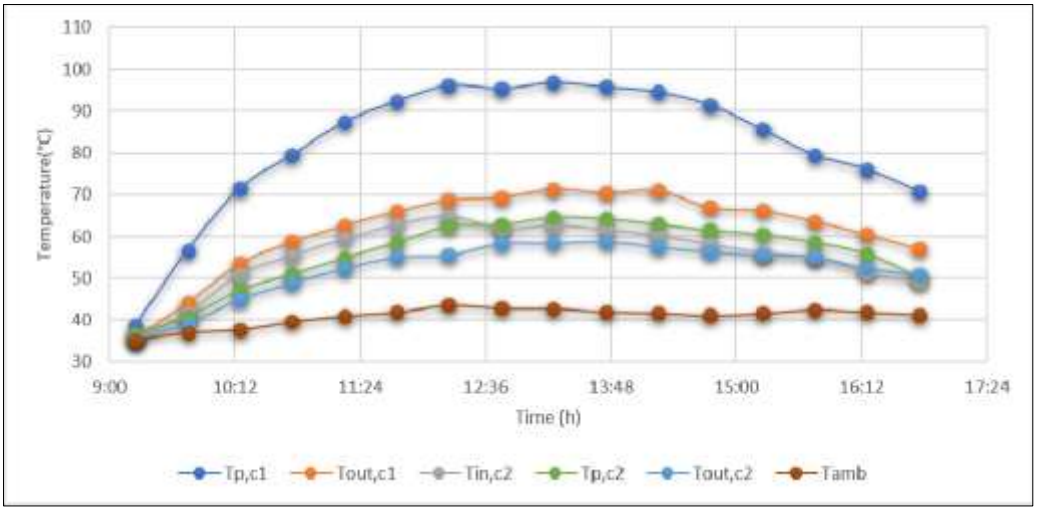


Figure V. 6: Temporal evolution of the temperature of the different components of the solar dryer with tubes (day 2)

The figure above represents the evolution of temperatures (°C) at various points of the dryer as a function of time (minutes) during the day of June 22. The curves present the same bell-shaped profile as the previous day, however with generally higher values.

- Regarding the primary collector (C_1), the absorber temperature $T_{p,c1}$ reaches a peak value of approximately 96 °C, reflecting the intense solar irradiance received by the tilted primary collector and the high absorptivity of the tubular absorber surface. The air outlet temperature $T_{out,c1}$ stabilises at approximately 72 °C at peak, representing a thermal elevation of approximately +28 °C (48%) above the ambient temperature (44°C). The relatively moderate gap between $T_{p,c1}$ and $T_{out,c1}$ (24 °C) compared to what was observed in the flat-plate configuration (35°C) confirms that the tubular absorber geometry significantly enhances convective heat transfer between the absorber surface and the working fluid, allowing the air to extract a greater fraction of the absorbed solar energy before exiting the collector.
- Wall-integrated secondary collector (C_2), the air enters C_2 already pre-heated at approximately 62 °C. A temperature drop of −10 °C is observed between $T_{out,c1}$ (72

°C) and $T_{in,c2}$ (65 °C). This difference is attributed to thermal losses within the flexible metallic duct connecting the two collectors, which acts as an unintended heat exchanger with the ambient environment. This avoidable thermal losses directly limits the inlet conditions of C_2 and reinforces the need for thermal insulation of the connecting duct as a priority design improvement.

- Comparing $T_{in,c2}$ and $T_{p,c2}$, two-phase thermal behaviour of the secondary collector C_2 is observed. The cylindrical geometry of the tubular absorber and its interaction with both the incident solar radiation and the pre-heated airflow arriving from C_1. Due to the cylindrical shape of the tubes, only the upper half of each tube is directly exposed to solar radiation and therefore absorbs the incident flux efficiently, reaching elevated temperatures. The lower half of the tubes, however, is shielded from direct solar irradiance and receives heat exclusively through thermal conduction from the upper exposed surface. As a result, the lower portion of the tubular absorber operates at a significantly lower temperature than the upper surface, creating a non-uniform radial temperature distribution within each tube.

During the morning phase, the hot air arriving from C_1 encounters the lower portion of the C_2 tubes, which is still relatively cool due to its limited solar exposure. Rather than being further heated, the incoming air transfers a fraction of its thermal energy to this cooler lower surface, which acts as a thermal storage element absorbing and accumulating heat from the airflow rather than releasing it. This heat absorption by the lower tube surface explains the observed reduction in air temperature as it passes through C_2 during the morning period, with $T_{p,c2}$ remaining below $T_{in,c2}$.

During the afternoon phase, once the lower portion of the tubular absorber has accumulated sufficient thermal energy and reached thermal saturation, it begins to release the stored heat back to the airflow. The absorber temperature $T_{p,c2}$ consequently rises above the inlet air temperature $T_{in,c2}$, and C_2 transitions from a heat sink into a supplementary heat source, contributing positively to the thermal elevation of the drying air. This transition corresponds precisely to the inversion observed in the curves after solar noon, where $T_{p,c2}$ exceeds $T_{in,c2}$ and the heat transfer direction is reversed.

The cylindrical tubular absorber of C_2 exhibits an intrinsic thermal storage and release behaviour driven by its geometry, which introduces a characteristic time lag between heat absorption in the morning and heat release in the afternoon. While this behaviour limits the immediate thermal contribution of C_2 during peak irradiance hours, it provides a valuable supplementary heating effect during the afternoon decline of solar radiation, partially

compensating for the reduced output of the primary collector C_1 at that time of day.

V.7. Evolution of Product Mass

The evolution of product mass during drying is the direct indicator of process efficiency. The results obtained for banana and mint during the days of June 18 and June 22 are presented below.

A. Banana

Figure V.7 presents the temporal evolution of banana mass for three drying configurations during the drying experiments conducted on 18th June (banane 1: flat-plate absorber, banane3: open-air reference tray) and 22nd June (banane 2: tubular absorber), all starting from an initial mass of approximately 205–208 g.

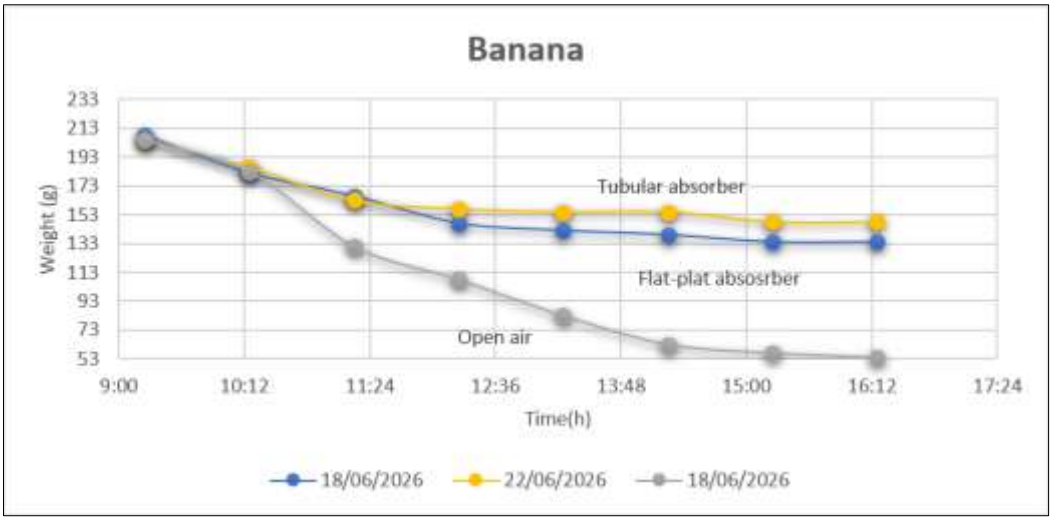


Figure V. 7: Hourly Evolution of the mass of bananas during the drying process

All curves exhibit a continuous decreasing trend reflecting progressive moisture evaporation throughout the session.

The open-air reference tray (18th June) achieved the highest mass loss of 71.9% (203 g → 57 g), owing to direct solar exposure and natural wind convection, though without any protection against contamination. The solar dryer with flat-plate absorber (18th June) yielded a mass loss of 36.5% (208 g → 132 g), while the tubular absorber configuration (22nd June) produced a lower apparent mass loss of 27.8% (205 g → 148 g). However, this seemingly inferior result must be interpreted with caution, as the significantly higher ambient temperature on 22nd June (44 °C vs. 30 °C) increased the relative humidity of the drying air, reducing its moisture-carrying capacity and limiting the evaporation rate.

B. Mint

Figure V.8 presents the temporal evolution of mint leaf mass for two drying configurations starting from initial masses of 63 g and 65 g respectively. Both curves exhibit a continuous decreasing trend reflecting progressive moisture evaporation throughout the session. The flat-plate absorber configuration (18th June) achieved a mass loss of 46% (63 g → 34 g), while the tubular absorber configuration (22nd June) yielded a lower apparent mass loss of 32.3% (65 g → 44 g). As with the banana results, this difference must be interpreted with caution due to the significantly higher ambient temperature on 22nd June (44 °C vs. 30 °C), which increased atmospheric humidity and consequently reduced the moisture-carrying capacity of the drying air, limiting the evaporation rate and despite the superior thermal performance of the tubular absorber.

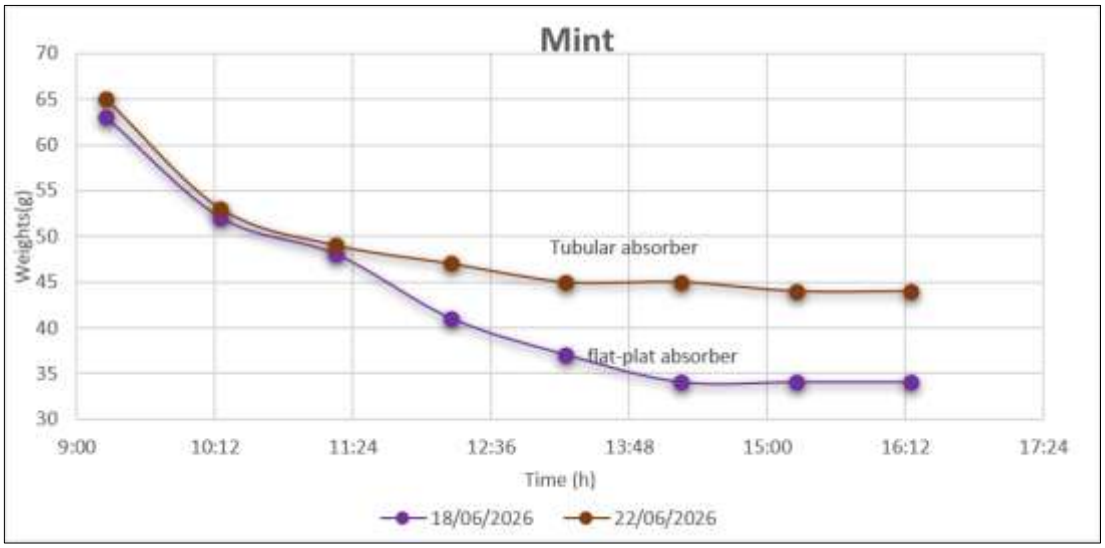


Figure V. 8: Hourly Evolution of the mass of mint during the drying process

V.8. Product after drying

In order to evaluate the effect of each drying configuration on the final product quality, a visual comparison was carried out on both banana slices and mint leaves after drying. The table below presents the appearance of the dried products under the three drying conditions.

As shown in the table, the open-air dried banana slices exhibited significant darkening and oxidation, resulting from prolonged direct exposure to sunlight and dust contamination. In contrast, the flat-plate absorber configuration (18th June) produced banana slices with a more uniform light brown color and an acceptable texture. The tubular absorber configuration (22nd June) yielded the lightest color among the three cases, indicating a more controlled and efficient drying process.

Regarding mint leaves, the open-air dried sample showed yellowing and loss of its characteristic green color, suggesting chlorophyll degradation due to excessive direct solar radiation. The flat-plate absorber preserved the green color to a moderate extent, while the tubular absorber maintained the best color retention among all configurations.

Overall, indirect solar drying proved superior in preserving the color, texture, and organoleptic qualities of both products compared to open-air drying, confirming the effectiveness of the solar drying system developed in this study.

Table V.1: Appearance of the dried products under the three drying conditions

	Banana slices	**Mint leaves**
Open-air drying (18th June)		
Flat-plate absorber (18th June)		
Tubular absorber (22nd June)		

V.9. Conclusion

This chapter presented the outdoor experimental investigation of the complete solar drying system, comprising the primary solar collector coupled with the active-wall drying chamber, tested under real solar irradiance conditions at the University of Tlemcen during

June. The experimental campaign was organised into two successive tests using banana slices and mint leaves, tested successively with the flat-plate and tubular absorber configurations.

- **Collector (C_1) :**

- The tubular absorber configuration achieved an air outlet temperature of 72 °C compared to 54 °C for the flat-plate design, representing a thermal improvement of +33.3% in outlet air temperature.
- The absorber temperature $T_{p,c1}$ reached up to 96 °C with the tubular configuration, confirming strong solar energy absorption under real outdoor conditions.
- The reduced gap between $T_{p,c1}$ and $T_{out,c1}$ in the tubular case confirms that the metallic tubes significantly enhance convective heat transfer between the absorber surface and the working fluid.

- **Active wall (C_2)**

- In the flat-plate configuration, the air experienced a temperature reduction of −7.4% between $T_{out,c1}$ and $T_{out,c2}$, indicating modest but limited thermal losses within C_2.
- In the tubular configuration, this reduction increased significantly to −20.8%, as the highly pre-heated air arriving from C_1 (72 °C) exceeded the C_2 absorber temperature (65 °C), causing C_2 to act as a heat dissipator rather than a supplementary heat source.
- These results reveal a fundamental limitation of the current serial airflow arrangement, particularly when C_1 operates at high efficiency.

- **Proposed solution: Circuit inversion:**

- A circuit inversion is strongly recommended as a priority design improvement: redirecting the airflow so that cold ambient air enters C_2 first, then C_1, before entering the drying chamber ($T_{amb} \rightarrow C_2 \rightarrow C_1 \rightarrow$ chamber).
- This modification would ensure a large positive temperature driving force within C_2 allowing both collectors to contribute positively and simultaneously to air heating.
- The inverted circuit is expected to significantly increase the total air temperature at the drying chamber inlet and improve the overall thermal efficiency of the integrated system.

- **Drying performance: Banana slices:**

- Open-air reference tray (18th June): mass loss of 71.9% highest drying rate due to direct solar exposure, but without any product protection against contamination.
- Flat-plate absorber (18th June): mass loss of 36.5%
- Tubular absorber (22nd June): mass loss of 27.8%
- The lower apparent performance of the tubular configuration is attributed to the higher ambient temperature on 22nd June (44 °C vs. 30 °C), which increased atmospheric humidity and reduced the moisture-carrying capacity of the drying air.

- **Drying performance: Mint leaves:**

- Flat-plate absorber (18th June): mass loss of 46%
- Tubular absorber (22nd June): mass loss of 32.3%
- The same environmental limitations apply, making a direct comparison between the two configurations inconclusive.
- Comparing the product after drying, indirect solar drying proved superior in preserving the color and texture of both products compared to open-air drying, confirming the effectiveness of the solar drying system developed in this study.

General conclusion

This master's thesis presented an experimental investigation of an innovative indirect forced-convection solar dryer integrating an active-wall concept, in which the sun-facing lateral wall of the drying chamber is replaced by a wall-integrated flat-plate air solar collector.

This design modification transforms a conventionally passive wooden wall into an active thermal component, enabling the recovery and valorisation of solar energy that would otherwise be lost through the dryer envelope, and providing supplementary heating to the drying air in series with the primary collector. The experimental investigation was conducted in two distinct phases: a controlled laboratory phase using a solar simulator to characterise the thermal performance of the active wall under reproducible conditions, and an outdoor experimental phase conducted at the University of Tlemcen in June, under real solar irradiance conditions, to evaluate the complete integrated drying system.

- **Laboratory experiments:**

- The flat-plate absorber achieved a maximum thermal efficiency of 68% under optimal conditions ($\dot{m}$ = 0.015 kg/s, I = 330 W/m²), with an optimal flow rate identified at 0.015 kg/s.
- The tubular absorber configuration consistently outperformed the flat-plate design across all tested conditions, achieving a peak thermal efficiency of 72%, a gain of +4%.
- The absorber temperatures were systematically reduced with the tubular configuration, with T_1 decreasing by −6 °C, confirming enhanced convective heat extraction and more uniform heat distribution along the absorber surface.
- The tubular absorber exhibited a continuously increasing efficiency with flow rate reaching 72.5% at 0.017 kg/s compared to the bell-shaped response of the flat-plate design, demonstrating a broader and more robust optimal operating range.
- The most significant efficiency gain was recorded at the lowest flow rate of 0.012 kg/s, where the tubular configuration achieved 67.5% compared to only 53% for the flat-plate design an absolute improvement of +14.5 %.

- **Outdoor experiments:**

- The primary collector (C_1) delivered outlet air temperatures of 54 °C (flat-plate, 18th June) and 72 °C (tubular, 22nd June), representing a thermal improvement of +33.3% attributable to the combined effect of the tubular geometry and the higher ambient temperature on 22nd June.
- The wall-integrated secondary collector (C_2) exhibited a limited thermal contribution under the current serial airflow arrangement, with the air experiencing temperature reductions of −7.4% (flat-plate) and −20.8% (tubular) between the C_1 and C_2 outlets, due to the pre-heated air arriving at temperatures exceeding the C_2 absorber temperature.
- Banana slices achieved mass losses of 36.5% (flat-plate, 18th June) and 27.8% (tubular, 22nd June), while mint leaves recorded mass losses of 46% and 32.3% respectively; the lower apparent drying performance of the tubular configuration on 22nd June is primarily attributed to the higher ambient temperature (44 °C vs. 30 °C), which increased atmospheric humidity and reduced the moisture-carrying capacity of the drying air.
- The open-air reference tray achieved the highest banana mass loss of 71.9%, confirming the strong evaporative potential of direct solar exposure, albeit without product protection.
- Comparing the product after drying, indirect solar drying proved superior in preserving the color, texture, and organoleptic qualities of both products compared to open-air drying, confirming the effectiveness of the solar drying system developed in this study.

- **Recommendations and perspectives:**

- A circuit inversion ($T_{amb} \rightarrow C_2 \rightarrow C_1 \rightarrow$ chamber) is strongly recommended as the most critical design improvement, ensuring that both collectors contribute positively to air heating by maximising the temperature driving force within C_2
- Enhanced thermal insulation of the flexible connecting duct between C_1 and C_2 is essential to minimise parasitic heat losses between the two collectors
- Same-day controlled testing under identical environmental conditions is necessary to draw definitive conclusions on the relative drying performance of the two absorber configurations.

- Future work should investigate the system performance under loaded drying conditions with a wider range of agricultural products, and explore the integration of thermal energy storage to extend the drying period beyond daylight hours

References

[1] Process Sensing, "Measurement of Water Activity (Aw) and Drying Rate," [Online]. Available: https://www.processsensing.com/fr-fr/blog/aw-mesure.htm [Accessed: 2024].

[2] F. P. Incropera, D. P. DeWitt, T. L. Bergman, and A. S. Lavine, *Fundamentals of Heat and Mass Transfer*, 7th ed. Hoboken, NJ: Wiley, 2011.

[3] N. Midoun and B. Kholkhal, "Amélioration des performances d'un séchoir solaire à capteur plan," Master's dissertation, Dept. Mechanical Engineering, Univ. of Tlemcen, Tlemcen, Algeria, 2024.

[4] A. Mouafki, "Modélisation-simulation du procédé de séchage solaire des feuilles de menthe," Master's dissertation, Dept. Engineering, Univ. of Ouargla, Ouargla, Algeria, 2004.

[5] A. Bareen, S. Dash, P. Kalita, and K. K. Dash, "Experimental investigation of an indirect solar dryer with PCM-integrated solar collector as a thermal energy storage medium," *Environmental Science and Pollution Research*, vol. 31, no. 12, pp. 18209–18225, 2024. https://doi.org/10.1007/s11356-023-26690-2

[6] N. Vijayaregunathan, V. Periyasamy, A. Munimathan *et al.*, "Experimental and exergy evaluation of a PCM integrated active indirect solar dryer for Turkey berries with economic and environmental assessment," *Scientific Reports*, vol. 15, p. 21661, 2025. https://doi.org/10.1038/s41598-025-02549-z

[7] M. Yazici and R. Kose, "Energy, exergy and economic investigation of novel hybrid dryer, indirect solar dryer and traditional shade drying," *Thermal Science and Engineering Progress*, vol. 49, p. 102502, 2024. https://doi.org/10.1016/j.tsep.2024.102502

[8] Q. Mawire, M. Ramokali, M. Mothupi, and M. Vanierschot, "An experimental evaluation of drying banana slices using a novel indirect solar dryer under variable conditions," *Heliyon*, vol. 10, no. 7, p. e28268, 2024. https://doi.org/10.1016/j.heliyon 2024.e28268

[9] M. M. Rafiq, S. Vasanthi, and S. Nagalakshmi, "Modeling and control of an indirect solar dryer in forced convection mode using system identification and model predictive control," *Electric Power Components and Systems*, 2024. https://doi.org/10.1080/15325008.2024.2316257

[10] B. B. Sharma, P. Vaidya, N. Kumar *et al.*, "Enhancing post-harvest sustainability in temperate crops through smart IoT-integrated indirect solar dryer," *Scientific Reports*, vol. 15, p. 28608, 2025. https://doi.org/10.1038/s41598-025-13499-x

[11] M. Zeeshan *et al.*, "Novel design and performance evaluation of an indirectly forced convection desiccant integrated solar dryer for drying tomatoes in Pakistan," *Heliyon*, vol. 10, no. 8, p. e29284, 2024. https://doi.org/10.1016/j.heliyon 2024.e29284

[12] M. Hossaine *et al.*, "Design, fabrication, and performance evaluation of an indirect solar-powered vegetable dryer," *ScienceDirect*, 2025. https://doi.org/10.1016/j.xxx.2025

[13] S. Touré, A. C. Ogo, and M. Sidibé, "Experimental study and thermal modelling of cocoa shell convective drying in an indirect solar dryer," *Modelling and Numerical Simulation of Material Science*, vol. 14, no. 2, 2024. https://doi.org/10.4236/mnsms.2024.142004

[14] M. Kaveh, Z. Parhizi, I. Golpour, M. Szymanek, A. M. Blanco-Marigorta, and Y. Darvishi, "Performance evaluation of solar drying chambers and drying kinetics of apple slices," *Energy for Sustainable Development*, 2025. https://doi.org/10.1016/j.esd.2025

Abstract-This work presents an experimental investigation of an indirect forced-convection solar dryer incorporating an innovative active-wall concept, in which the sun-facing wall of the drying chamber is replaced by a wall-integrated flat-plate air solar collector, enabling the recovery of solar energy otherwise lost through the dryer envelope. Two absorber configurations were tested: a flat-plate absorber and a tubular absorber integrating parallel rough-surfaced aluminium tubes. Laboratory tests demonstrated that the tubular configuration achieves a superior thermal efficiency of 72% versus 68% for the flat-plate design, with a more uniform temperature distribution and a broader optimal operating range. The complete solar drying system comprising the primary collector coupled with the active-wall chamber was subsequently tested outdoors at the University of Tlemcen in June, under real solar irradiance conditions, using banana slices and mint leaves as drying products. Outdoor experiments confirmed the operational feasibility of the system, with the primary collector delivering outlet temperatures of 54 °C and 72 °C for the flat-plate and tubular configurations respectively. However, the wall-integrated secondary collector exhibited a limited thermal contribution under the current serial airflow arrangement, as the pre-heated air arriving from the primary collector frequently exceeded the secondary absorber temperature, resulting in a net heat loss. A circuit inversion ($T_{amb} \rightarrow C_2 \rightarrow C_1 \rightarrow$ chamber) is proposed as a priority design improvement to address this limitation.

Résumé-Ce travail présente une étude expérimentale d'un séchoir solaire indirect à convection forcée intégrant un concept innovant de paroi active, dans lequel la paroi exposée au soleil de la chambre de séchage est remplacée par un capteur solaire plan à air intégré directement à la paroi, permettant la récupération de l'énergie solaire autrement perdue à travers l'enveloppe du séchoir. Deux configurations d'absorbeur ont été testées : un absorbeur plan lisse servant de configuration de référence, et un absorbeur tubulaire intégrant un réseau de tubes en aluminium à surface rugueuse disposés en parallèle. Les essais en laboratoire ont démontré que la configuration tubulaire atteint un rendement thermique supérieur de 72% contre 68% pour l'absorbeur plan, avec une distribution de température plus uniforme le long de la surface absorbante et une plage de fonctionnement optimal plus large. Le système de séchage solaire complet comprenant le capteur principal couplé à la chambre à paroi active a ensuite été testé en extérieur à l'Université de Tlemcen au mois de juin, sous rayonnement solaire réel, en utilisant des tranches de banane et des feuilles de menthe comme produits à sécher. Les expériences en extérieur ont confirmé la faisabilité opérationnelle du système, le capteur principal délivrant des températures de sortie de 54 °C et 72 °C pour les configurations à absorbeur plan et tubulaire respectivement. Cependant, le capteur secondaire intégré à la paroi a présenté une contribution thermique limitée dans la configuration actuelle d'écoulement en série, l'air préchauffé provenant du capteur principal dépassant fréquemment la température de l'absorbeur secondaire, entraînant une perte thermique nette. Une inversion du circuit ($T_{amb} \rightarrow C_2 \rightarrow C_1 \rightarrow$ chambre) est proposée comme amélioration prioritaire pour remédier à cette limitation.

الملخص - تقدم هذه الدراسة تحقيقًا تجريبيًا لمجفف شمسي غير مباشر بالحمل الحراري القسري، يتضمن مفهومًا مبتكرًا يُعرف بـ"الجدار النشط، حيث يتم استبدال الجدار المواجه للشمس في غرفة التجفيف بمجمع شمسي مستوٍ للهواء مدمج مباشرةً في الجدار، مما يتيح استرداد الطاقة الشمسية التي كانت تُفقد عبر غلاف المجفف. تم اختبار تصميمين مختلفين للماص :ماص مستوٍ أملس يمثل
التصميم المرجعي، وماص أنبوبي يضم مجموعة من الأنابيب الألومينيوم ذات السطح الخشن المرتبة بشكل متوازٍ. أثبتت الاختبارات المخبرية أن التصميم الأنبوبي يحقق كفاءة حرارية أعلى بلغت 72%مقارنةً بـ 68% للتصميم المستوي، مع توزيع أكثر انتظامًا لدرجات الحرارة على طول سطح الماص ونطاق تشغيل مثالي أوسع. وقد خضع نظام التجفيف الشمسي الكامل المكوّن من المجمع الرئيسي المقترن بغرفة الجدار النشط لاختبارات ميدانية في جامعة تلمسان خلال شهر جوان، تحت ظروف الإشعاع الشمسي الحقيقي، باستخدام شرائح الموز وأوراق النعناع منتجات للتجفيف. أكدت التجارب الميدانية الجدوى التشغيلية للنظام، إذ حقق المجمع
الرئيسي درجات حرارة عند المخرج بلغت 54°C و 72 °C للتصميمين المستوي والأنبوبي على التوالي. غير أن المجمع الثانوي المدمج في الجدار أظهر مساهمة حرارية محدودة في التكوين الحالي للتدفق التسلسلي، إذ كانت درجة حرارة الهواء المسخّن مسبقًا القادم من المجمع الرئيسي تتجاوز في أغلب الأحيان درجة حرارة الماص الثانوي، مما أدى إلى فقدان حراري صافٍ. ولمعالجة هذه المحدودية، يُقترح عكس دائرة تدفق الهواء ← $C_1 \rightarrow C_2 \rightarrow T_{amb}$) غرفة التجفيف كتحسين تصميمي ذي أولوية

REPUBLIQUE ALGERIENNE DEMOCRATIQUE ET POPULAIRE
Ministère de l'Enseignement Supérieur et de la Recherche Scientifique

Université Abou Bekr Belkaid Tlemcen

Business Model Canvas

BMC

Date de dépôt :2/07/2026

N° de projet :1 Label

Faculté/Institut :de technologie

Département : Génie mécanique

Nom du projet : Étude de la conception et de la fabrication d'un séchoir solaire indirect

Encadrant 1: Khaldi Souheyla

Co-encadrant 1: Sarri Hassoun Hind

Etudiants : - BENKOU Naila -

- BENKATI Bouchra -

Année universitaire : 2025/2026

1- Proposition de valeur (Value Proposition)القيمة المقترحة

a. Quels problèmes résolvons-nous pour nos clients ?

ما هي المشاكل التي نحلها لعملائنا ؟

Notre séchoir solaire indirect permet de résoudre les problèmes liés au coût élevé du séchage conventionnel, à la dépendance aux énergies non renouvelables, ainsi qu'à la mauvaise qualité des produits séchés au soleil direct (pertes nutritionnelles et risques de contamination). Il offre également une solution pour réduire le temps de séchage, mieux contrôler le procédé et limiter les pertes post-récolte, tout en restant économique, écologique et adaptée au contexte local.

b. Quels besoins de nos clients satisfont nos produits ou services ?

ما هي الاحتياجات التي يلبيها منتجاتنا أو خدماتنا لعملائنا؟

Il répond au besoin de conserver les produits agricoles plus longtemps, d obtenir une meilleure qualité de séchage , de réduire les pertes après récolte et de diminuer les coûts énergétique grâce a l utilisation de l énergie solaire.

c. En quoi notre offre est-elle différente de celle de nos concurrents ?

في ماذا تختلف عروضنا عن تلك التي يقدمها منافسونا؟

Notre séchoir se distingue par conception innovante utilisant une paroi améliorée avec des tubes flexibles qui augment le transfert thermique et améliorent l efficacité du séchage tout en préservant la qualité des produits.

d. Quelles est notre proposition unique de valeur ?

ما هو العرض الفريد للقيمة لدينا؟

Offrir un séchoir solaire indirect écologique, économique et performant, capable de produire des fruits et légumes séchés de meilleure qualité avec un temps de séchage réduit et une faible consommation d énergie

2- Segments de clients (Customer Segment) انواع العملاء :

a. Quels sont nos clients principaux?

من هم العملاء او الزبائن الرئيسيون ؟

Nos principaux clients sont les agriculteurs, les coopératives agricoles, les producteurs de fruits, légumes et plantes médicinales, les petites entreprises agroalimentaires, ainsi que les centres de recherche et les organismes de développement rural recherchant une solution de séchage économique, écologique et utilisant l'énergie solaire.

b. Quels sont les différents segments de clients que nous visons ?

ما هي الفئات المختلفة من العملاء التي تستهدفها؟

Les segments de clients visés comprennent les petits et grands agriculteurs, les coopératives agricoles, les producteurs de fruits, légumes et plantes médicinales, les entreprises agroalimentaires, les centres de recherche et de formation, ainsi que les organisations de développement rural et les entrepreneurs intéressés par les technologies de séchage solaire. Ces

clients recherchent des solutions efficaces, économiques et respectueuses de l'environnement pour la conservation des produits agricoles.

c. Quels sont les besoins spécifiques de chaque segment de clients?
ما هي الاحتياجات الخاصة لكل فئة من العملاء؟

Chaque segment de clients possède des besoins spécifiques. Les agriculteurs recherchent principalement la réduction des pertes post-récolte et une meilleure conservation des produits. Les coopératives et les entreprises agroalimentaires ont besoin d'une capacité de séchage plus importante et d'une qualité de produit constante. Les producteurs de fruits, légumes et plantes médicinales souhaitent préserver les qualités nutritionnelles et organoleptiques de leurs produits. Les centres de recherche utilisent le séchoir à des fins expérimentales, tandis que les ONG recherchent une solution durable, économique et adaptée au développement rural.

d. Comment pouvons-nous catégoriser nos clients en groupes distincts?
كيف يمكن تصنيف عملائنا الى مجموعات مختلفة؟

Nos clients peuvent être regroupés en quatre catégories principales : le secteur agricole (agriculteurs, coopératives et producteurs agricoles), le secteur agroalimentaire (entreprises de transformation des produits agricoles), le secteur de la recherche et de l'enseignement (universités et centres de recherche) et le secteur du développement rural (ONG et associations). Cette classification permet d'adapter les caractéristiques du séchoir solaire indirect aux besoins spécifiques de chaque groupe de clients.

3- Relation avec les clients (Consumer Relationships) علاقة مع العملاء :

a. Quel type de relation chaque segment de clients attend il de nous ?
اي نوع من العلاقة يتوقعه كل فئة من العملاء منا؟

Chaque segment de clients attend une relation adaptée à ses besoins. Les agriculteurs recherchent principalement un accompagnement technique et une formation à l'utilisation du séchoir solaire. Les coopératives et les entreprises agroalimentaires attendent un suivi personnalisé, un service après-vente efficace et une assistance technique continue. Les centres de recherche privilégient une collaboration scientifique et un soutien technique spécialisé, tandis que les ONG recherchent un partenariat durable favorisant le développement rural et l'adoption de technologies écologiques..

b. Comment entretenons-nous actuellement les relations avec nos clients ?
كيف نحافظ حاليًا على العلاقات مع عملائنا؟

Nous entretenons actuellement les relations avec nos clients grâce à un contact direct et personnalisé. Nous assurons un accompagnement technique lors de l'installation et de l'utilisation du séchoir solaire indirect, ainsi qu'un suivi régulier pour garantir son bon fonctionnement. Nous restons également disponibles pour répondre aux questions, fournir une assistance technique et recueillir les retours des utilisateurs afin d'améliorer continuellement notre solution.

c. Comment pouvons-nous améliorer ou personnaliser nos interactions avec nos clients ?

كيف يمكننا تحسين أو تخصيص تفاعلاتنا مع عملائنا؟

Nous pouvons améliorer nos interactions avec les clients en proposant un accompagnement personnalisé, des formations adaptées et un service après-vente réactif. Un suivi régulier, l'utilisation de moyens de communication modernes et la prise en compte des retours des utilisateurs permettront de renforcer la satisfaction et la fidélité des clients. De plus, l'adaptation du séchoir solaire indirect aux besoins spécifiques de chaque client contribuera à établir une relation durable et de confiance.

4- Canaux de distribution (Channels) قنوات التوزيع :

a- Par quels canaux nos clients veulent-ils être atteints ?

من خلال أي قنوات يفضل عملاؤنا أن يتم التواصل معهم؟

Nos clients souhaitent être atteints principalement par des canaux de communication simples, efficaces et accessibles. Le contact direct sur le terrain constitue un moyen privilégié pour présenter le fonctionnement du séchoir solaire indirect et répondre aux besoins spécifiques des utilisateurs. Le téléphone et l'e-mail permettent d'assurer un suivi rapide et un support technique continu. Les réseaux sociaux facilitent la diffusion d'informations, la promotion du produit et les échanges avec les clients. La participation à des foires et salons agricoles ainsi que la collaboration avec les coopératives et associations agricoles représentent également des canaux importants pour faire connaître la solution à un public plus large. Enfin, un site web dédié peut servir de plateforme d'information et de communication pour les clients actuels et potentiels.

b- Quels canaux sont les plus efficaces pour atteindre chaque segment de clients ?

ما هي القنوات الأكثر فعالية للوصول إلى كل فئة من العملاء؟

Les canaux les plus efficaces varient selon chaque segment de clients. Les petits agriculteurs sont mieux atteints par le contact direct sur le terrain, les démonstrations et les coopératives agricoles. Les grandes exploitations et coopératives préfèrent les réunions techniques, les salons agricoles et les communications professionnelles par e-mail. Les entreprises agroalimentaires utilisent principalement les canaux numériques et les rendez-vous B2B. Les centres de recherche et universités privilégient les collaborations scientifiques et les échanges académiques, tandis que les ONG et organismes de développement

rural sont atteints efficacement par des partenariats institutionnels et des projets de terrain.

c- Comment pouvons-nous intégrer différents canaux pour améliorer l'expérience clients ?

كيف يمكننا دمج مختلف القنوات لتحسين تجربة العملاء؟

Nous pouvons intégrer différents canaux en assurant une communication cohérente et continue entre tous les points de contact avec les clients. L'objectif est de permettre au client de passer facilement d'un canal à un autre (terrain, téléphone, e-mail ou réseaux sociaux) tout en gardant le même niveau d'information et de service. La centralisation des données clients dans un système unique, ainsi que la coordination entre les équipes techniques et commerciales, permet d'améliorer la réactivité et la qualité du service. Cette approche multicanale garantit une meilleure expérience utilisateur et renforce la satisfaction des clients.

5- Partenaires clés (Key Partnerships) : الشراكة الرئيسية

a. Qui sont nos partenaires clés ?

من هم شركاؤنا الرئيسيون؟

Nos partenaires clés sont les fournisseurs de matériaux et d'équipements, les artisans et entreprises de fabrication, les centres de recherche et universités, les coopératives agricoles, les ONG et organismes de développement rural, ainsi que les institutions publiques et les distributeurs spécialisés. Ces partenaires jouent un rôle essentiel dans la conception, la fabrication, la diffusion et l'amélioration du séchoir solaire indirect.

b. Quels sont les partenariats qui nous aident à réduire les coûts, à accéder à de nouvelles ressources ou à améliorer notre proposition de valeur ?

ما هي الشراكات التي تساعدنا على خفض التكاليف أو الوصول إلى موارد جديدة أو تحسين قيمتنا المقترحة؟

Les partenariats avec les fournisseurs de matériaux permettent de réduire les coûts d'approvisionnement, tandis que les coopératives agricoles facilitent l'accès aux clients et diminuent les coûts de distribution. Les universités et centres de recherche contribuent à l'amélioration de la technologie et de la performance du séchoir solaire. Les ONG et les programmes de développement offrent un soutien financier et logistique, et les institutions publiques peuvent apporter des subventions et un appui institutionnel. Enfin,

les artisans locaux permettent de réduire les coûts de fabrication tout en adaptant le produit aux besoins du marché local.

c. Comment pouvons-nous aligner nos intérêts avec ceux de nos partenaires ?

كيف يمكننا مزامنة مصالحنا مع تلك لشركائنا؟

Nous pouvons aligner nos intérêts avec ceux de nos partenaires en définissant des objectifs communs tels que la réduction des pertes agricoles et la promotion des énergies renouvelables. Il est important d'établir des accords gagnant-gagnant, de partager les bénéfices et de collaborer dans la recherche et le développement afin d'améliorer le séchoir solaire indirect. Une communication régulière, une implication des partenaires dans les décisions et la mise en place de projets pilotes permettent également de renforcer la confiance et d'assurer une coopération durable et efficace.

6- Activités clés (Key Activities) :الأنشطة الرئيسية

a. Quelles sont les actions principales que nous devons entreprendre pour livrer notre proposition de valeur ?

ما هي الأنشطة الرئيسية التي يجب علينا القيام بها لتقديم قيمتنا المقترحة؟

Les principales activités consistent à concevoir et améliorer le séchoir solaire indirect, fabriquer et assembler ses composants, puis assurer son installation chez les clients. Nous réalisons également des tests de performance et un contrôle de qualité afin de garantir l'efficacité du séchage. Par ailleurs, nous assurons la formation des utilisateurs, la maintenance et le service après-vente. Enfin, la recherche et développement ainsi que la gestion de la chaîne d'approvisionnement sont essentielles pour améliorer continuellement la proposition de valeur.

b. Quelles sont les opérations essentielles pour notre entreprise ?

ما هي العمليات الأساسية لشركتنا؟

Les opérations essentielles de notre entreprise comprennent la conception technique du séchoir solaire indirect, l'approvisionnement en matières premières, ainsi que la fabrication et l'assemblage des équipements. Elles incluent également le contrôle qualité, l'installation chez les clients, la maintenance et le service après-vente. À cela s'ajoutent la gestion des ventes, le suivi des clients et l'amélioration continue du produit afin de garantir sa performance et sa fiabilité.

c. Quelles sont les activités qui créent le plus de valeur pour nos clients ?

ما هي الأنشطة التي تخلق أكبر قيمة لعملائنا؟

Les activités qui créent le plus de valeur pour nos clients sont principalement la conception d'un séchoir solaire performant assurant un séchage efficace et homogène, ainsi que son installation et sa mise en service adaptées aux besoins spécifiques de chaque utilisateur. La formation des clients, le service après-vente et la maintenance rapide jouent également un rôle essentiel dans la satisfaction des utilisateurs. Enfin, l'amélioration continue du système et le contrôle de la qualité du séchage permettent de garantir des produits finis de haute valeur nutritionnelle et commerciale.

7- Ressources clés (Key resources): الموارد الرئيسية

a. Quels sont nos actifs matériels, immatériels et humains essentiels ?

ما هي الأصول المادية وغير المادية والبشرية الأساسية لدينا؟

Nos actifs essentiels se répartissent en trois catégories. Les actifs matériels comprennent les machines, les outils de fabrication, les composants du séchoir solaire et les équipements de test et de transport. Les actifs immatériels incluent le savoir-faire technique, les plans et prototypes, l'expérience en optimisation énergétique ainsi que les relations avec les partenaires. Enfin, les actifs humains regroupent les ingénieurs, techniciens, équipes de production, d'installation, de maintenance et de gestion commerciale, qui assurent le bon fonctionnement et le développement du projet.

b. Quels sont les outils, les technologies ou les partenariats dont nous avons besoin pour réussir ?

ما هي الأدوات والتكنولوجيا أو الشراكات التي نحتاجها لتحقيق النجاح؟

- **Outils :**
  - Machines de fabrication et de découpe des métaux.
  - Outils d'assemblage et de soudure.
  - Instruments de mesure (température, humidité, débit d'air).
  - Logiciels de conception et de simulation (CAO).
- **Technologies :**
  - Technologie de séchage solaire indirect.
  - Systèmes de ventilation naturelle ou forcée.
  - Matériaux isolants thermiques performants.
  - Capteurs pour le suivi des performances.
- **Partenariats :**
  - Fournisseurs de matériaux (métal, verre, isolants).
  - Universités et centres de recherche pour l'innovation.

- Coopératives agricoles pour les tests et l'utilisation.
- ONG et programmes de développement pour le soutien et le financement.
- Institutions publiques pour l'appui et les subventions.

c. Quels sont les principaux avantages concurrentiels de nos ressources ?

ما هي المزايا التنافسية الرئيسية لمواردنا؟

Les principaux avantages concurrentiels de nos ressources reposent sur un savoir-faire technique local dans la conception du séchoir solaire indirect et l'utilisation de matériaux disponibles localement, ce qui permet de réduire les coûts. Nous disposons également d'une expérience dans les énergies renouvelables, offrant une meilleure efficacité énergétique. La flexibilité de conception permet d'adapter le produit aux différents besoins des clients. Enfin, notre réseau de partenaires, ainsi que la disponibilité d'une main-d'œuvre qualifiée, renforcent notre capacité d'innovation, de production et de diffusion, tout en proposant une solution écologique et économique compétitive.

8- Charges et coûts (Coste sructure) :التكاليف

a. Quels sont les coûts fixes et variables associés à notre modèle économique ?

ما هي التكاليف الثابتة والمتغيرة المرتبطة بنموذجنا الاقتصادي؟

Les coûts fixes de notre modèle économique comprennent la location ou la maintenance de l'atelier, les salaires du personnel permanent, l'amortissement des équipements, les frais administratifs ainsi que les dépenses liées à la recherche et développement. Les coûts variables sont principalement liés à la production et incluent l'achat des matières premières, les coûts de fabrication, le transport et l'installation chez les clients, ainsi que les consommables, les pièces de rechange et les services de formation et de support technique.

b. Quels sont les coûts les plus importants pour notre entreprise ?

ما هي التكاليف الأكثر أهمية لشركتنا؟

Les coûts les plus importants pour notre entreprise sont principalement ceux liés aux matières premières utilisées pour la fabrication du séchoir solaire indirect, ainsi que les coûts de fabrication et de main-d'œuvre. Les dépenses de transport et d'installation chez les clients représentent également une part importante. À cela s'ajoutent les coûts de recherche et développement pour améliorer la performance du système, ainsi que les coûts de maintenance et de service après-vente qui assurent la satisfaction et la fidélisation des clients..

c. Comment pouvons-nous réduire les coûts ou améliorer l'efficacité de nos opérations ?

كيف يمكننا خفض التكاليف أو تحسين كفاءة عملياتنا؟

- Optimiser la conception du séchoir pour réduire la consommation de matériaux et simplifier la fabrication.
- Utiliser des matériaux locaux et moins coûteux sans compromettre la qualité.
- Standardiser les composants pour faciliter la production en série et réduire le temps de fabrication.
- Améliorer l'organisation du travail dans l'atelier pour éviter les pertes de temps et les erreurs.
- Former le personnel afin d'augmenter la productivité et la qualité du travail.
- Réduire les coûts logistiques en privilégiant la fabrication et l'installation locales.
- Mettre en place une maintenance préventive pour éviter les pannes et les réparations coûteuses.
- Digitaliser certaines tâches (suivi des stocks, gestion des commandes) pour améliorer l'efficacité.

9- Revenus (Revenue) : مصادر الدخل

a. Quels produits ou services nos clients sont-ils prêts à payer ?

ما هي المنتجات أو الخدمات التي يكون عملاؤنا على استعداد لدفع ثمنها؟

- La vente du **séchoir solaire indirect** (équipement complet).
- Les services d'**installation et de mise en service**.
- La **maintenance et le service après-vente**.
- La **formation des utilisateurs**.
- La **personnalisation du séchoir** selon les besoins.
- La vente de **pièces de rechange et accessoires**.
- Les **services de conseil technique**.
- Et éventuellement la **vente de produits agricoles séchés** (fruits, légumes, plantes aromatiques ou médicinales).

b. Quels sont les différents moyens par lesquels nous pouvons générer des revenus ?

ما هي الطرق المختلفة التي يمكننا من خلالها تحقيق الدخل؟

Nous pouvons générer des revenus à travers plusieurs sources principales. Tout d'abord, la **vente du séchoir solaire** représente une source directe de revenu grâce à la commercialisation

de l'équipement. Ensuite, la **vente des produits séchés** (fruits, légumes, etc.) permet de créer un revenu régulier basé sur le prix au kilogramme. Nous pouvons également proposer un **service de séchage pour les agriculteurs** qui souhaitent sécher leurs produits sans acheter l'équipement. Enfin, il est possible de développer des revenus supplémentaires à travers la **maintenance, l'installation et la formation** des utilisateurs.

c. Quel est notre modèle de tarification ?

ما هو نموذج التسعير لدينا؟

Notre modèle de tarification repose principalement sur une approche simple combinant le **coût de production et une marge bénéficiaire**, afin d'assurer la rentabilité du projet. Pour les produits séchés, le prix est fixé **au kilogramme selon le type de produit et sa valeur sur le marché**, tout en restant compétitif par rapport à la concurrence et accessible aux clients.

Materiaux	**Quantité**	**Prix (DZD)**
Les tubes	6	6000.00
Tronçonneuse	1	700.00
Cornière 3.5×3.5 (demi lord15)	4	2200.00
Support	1	800.00
Relou de lain de roche 0.7m	3m	2400.00
Tube de colle silicone	1	330.00
Suport colle silicone(pistolet)	1	350.00
Tole(0.75m*0.59m)	1	3000.00
Le verre 5mm	1	2000.00
Le bois	4	9600.00
Ventilateur	1	1000.00
Peinture noir	1	400.00

Visseuse	1	13200.00
Scie sauteuse	1	14000.00
chignole	1	18000.00
Les tournevis	1	3500.00
Débarbeuse	1	9800.00
Contre paquet (multiplié) 1.2×2m	1	3500.00

- Coût net = 90780,00 DZD/unité
- Coût net = 90780,00*24 unités = 2178720,00 DZD/an
- Coût fixe = 80000,00 DZD/ mois
- Coût fixe = 80000,00*24 unités = 192000,00 DZD/ an

Cost revenue

- Prix de vente unitaire pour le séchoir = 120000,00 DZD
- Prix de vente d'une année = 120000,00*24 unités = 2880000,00 DZD
- Prix de vente pour 1 g de banane = 20,00 DZD
- La quantité vendue en 1 année = 5760000.00 DZD/ an
- Prix de vente pour 1 g de Menthe = 3 DZD
- La quentité vendue en 1 année = 864000.00 DZD

Business Model Canevas : BMC

Partenaires clés
Key Partnerships
الشراكة الرئيسي

Fournisseurs de matériaux (bois, tôle, vitrage, isolants).

Ateliers de fabrication et artisans locaux.

Institutions universitaires et laboratoires de recherche.

Agriculteurs locaux pour les essais et la validation du séchoir.

Activités clés
Key Activities
الأنشطة الرئيسية

Étude et conception du séchoir solaire indirect.

Fabrication et assemblage du prototype.

Réalisation des tests expérimentaux de séchage

Ressources clés
Key resources
الموارد الرئيسية

Matériaux de construction du séchoir.

Outils et équipements de fabrication.

Connaissances scientifiques et techniques.

Main-d'œuvre et temps de

Proposition de valeur
Value Proposition
القيمة المقترحة

Séchoir solaire indirect économique et écologique.

Amélioration de la qualité des produits séchés.

Réduction de la consommation d'énergie conventionnelle.

Solution adaptée aux zones rurales et agricoles.

Relation clients
Consumer Relationship
علاقة مع العملاء

Accompagnement et sensibilisation des utilisateurs.

Formation à l'utilisation et à l'entretien du séchoir.

Explication du fonctionnement technique du

Canaux de distribution
Channels
قنوات التوزيع

Vente directe aux agriculteurs et producteurs locaux.

Présentation lors des foires agricoles.

Coopératives agricoles

Segment client
Customer Segment
انواع العملاء

Agriculteurs et producteurs de fruits et légumes.

Petites exploitations rurales.

Coopératives agricoles.

Transformateurs de produits agroalimentaires.

Coûts
Coste sructure
التكاليف

Coût des matériaux de fabrication.
Coût de la main-d'œuvre.
Coût des tests et expérimentations.
Coût de maintenance du séchoir.

Revenus
Revenue
مصادر الدخل

Vente du séchoir solaire indirect.
Services de fabrication sur commande.
Vente de produits agricoles séchés.